ISSN 1949-8470 (online)

World Journal of *Radiology*

World J Radiol 2015 August 28; 7(8): 184-219

Published by Baishideng Publishing Group Inc

WJR World Journal of Radiology

A peer-reviewed, online, open-access journal of Radiology

Editorial Board

2014-2017

The *World Journal of Radiology* Editorial Board consists of 365 members, representing a team of worldwide experts in radiology. They are from 36 countries, including Afghanistan (1), Argentina (2), Australia (5), Austria (7), Belgium (2), Brazil (8), Canada (6), Chile (1), China (43), Croatia (1), Denmark (4), Egypt (6), France (5), Germany (22), Greece (10), India (12), Iran (6), Ireland (2), Israel (3), Italy (47), Japan (13), Netherlands (1), New Zealand (1), Pakistan (1), Poland (2), Portugal (1), Serbia (1), Singapore (3), Slovakia (1), South Korea (18), Spain (4), Sweden (2), Switzerland (4), Thailand (1), Turkey (26), United Kingdom (11), and United States (82).

Yue-Qi Zhu, *Shanghai*

Croatia

Goran Kusec, Osijek

Denmark

Poul E Andersen, *Odense*
Lars J Petersen, *Aalborg*
Thomas Z Ramsoy, *Frederiksberg*
Morten Ziebell, *Copenhagen*

Egypt

Mohamed F Bazeed, *Mansoura*
Mohamed Abou El-Ghar, *Mansoura*
Reem HA Mohamed, *Cairo*
Mohamed R Nouh, *Alexandria*
Ahmed AKA Razek, *Mansoura*
Ashraf A Zytoon, *Shebin El-Koom*

France

Sabine F Bensamoun, *Compiègne*
Romaric Loffroy, *Dijon*
Stephanie Nougaret, *Montpellier*
Hassane Oudadesse, *Rennes*
Vincent Vinh-Hung, *Fort-de-France*

Germany

Henryk Barthel, *Leipzig*
Peter Bannas, *Hamburg*
Martin Beeres, *Frankfurt*
Ilja F Ciernik, *Dessau*
A Dimitrakopoulou-Strauss, *Heidelberg*
Peter A Fasching, *Erlanegn*
Andreas G Schreyer, *Regensburg*
Philipp Heusch, *Duesseldorf*
Sonja M Kirchhoff, *Munich*
Sebastian Ley, *Munich*
Adel Maataoui, *Frankfurt am Main*
Stephan M Meckel, *Freiburg*
Hans W Muller, *Duesseldorf*
Kay Raum, *Berlin*
Dirk Rades, *Luebeck*
Marc-Ulrich Regier, *Hamburg*
Alexey Surov, *Halle*
Martin Walter, *Magdeburg*
Axel Wetter, *Essen*
Christoph Zilkens, *Düsseldorf*

Greece

Panagiotis Antoniou, *Thessaloniki*
Nikos Efthimiou, *Athens*
Dimitris Karnabatidis, *Patras*
George Latsios, *Athens*
Stylianos Megremis, *Iraklion*
Alexander D Rapidis, *Athens*
Kiki Theodorou, *Larissa*
Ioannis A Tsalafoutas, *Athens*
Evanthia E Tripoliti, *Ioannina*
Athina C Tsili, *Ioannina*

India

Ritesh Agarwal, *Chandigarh*
Chandan J Das, *New Delhi*
Prathamesh V Joshi, *Mumbai*
Naveen Kalra, *Chandigarh*
Chandrasekharan Kesavadas, *Trivandrum*
Jyoti Kumar, *New Delhi*
Atin Kumar, *New Delhi*
Kaushala P Mishra, *Allahabad*
Daya N Sharma, *New Delhi*
Binit Sureka, *New Delhi*
Sanjay Sharma, *New Delhi*
Raja R Yadav, *Allahabad*

Iran

Majid Assadi, *Bushehr*
SeyedReza Najafizadeh, *Tehran*
Mohammad Ali Oghabian, *Tehran*
Amir Reza Radmard, *Tehran*
Ramin Sadeghi, *Mashhad*
Hadi Rokni Yazdi, *Tehran*

Ireland

Tadhg Gleeson, *Wexford*
Frederik JAI Vernimmen, *Cork*

Israel

Dafna Ben Bashat, *Tel Aviv*
Amit Gefen, *Tel Aviv*
Tamar Sella, *Jerusalem*

Italy

Adriano Alippi, *Rome*
Dante Amelio, *Trento*
Michele Anzidei, *Rome*
Filippo F Angileri, *Messinas*
Stefano Arcangeli, *Rome*
Roberto Azzoni, *San Donato milanese*
Tommaso V Bartolotta, *Palermo*
Tommaso Bartalena, *Imola*
Livia Bernardin, *San Bonifacio*
Federico Boschi, *Verona*
Sergio Casciaro, *Lecce*
Emanuele Casciani, *Rome*
Musa M Can, *Napoli*
Alberto Cuocolo, *Napoli*
Michele Ferrara, *Coppito*
Mauro Feola, *Fossano*
Giampiero Francica, *Castel Volturno*
Luigi De Gennaro, *Rome*
Giulio Giovannetti, *Pisa*
Francesca Iacobellis, *Napoli*
Formato Invernizzi, *Monza Brianza*
Francesco Lassandro, *Naples*
Lorenzo Livi, *Florence*
Pier P Mainenti, *Napoli*
Laura Marzetti, *Chieti*
Giuseppe Malinverni, *Crescentino*
Enrica Milanesi, *Turin*
Giovanni Morana, *Treviso*
Lorenzo Monti, *Milan*
Silvia D Morbelli, *Genoa*
Barbara Palumbo, *Perugia*
Cecilia Parazzini, *Milan*
Stefano Pergolizzi, *Messina*
Antonio Pinto, *Naples*
Camillo Porcaro, *Rome*
Carlo C Quattrocchi, *Rome*
Alberto Rebonato, *Perugia*
Giuseppe Rizzo, *Rome*
Roberto De Rosa, *Naples*
Domenico Rubello, *Rovigo*
Andrea Salvati, *Bari*
Sergio Sartori, *Ferrara*
Luca M Sconfienza, *Milano*
Giovanni Storto, *Rionero*
Nicola Sverzellati, *Parma*
Alberto S Tagliafico, *Genova*
Nicola Troisi, *Florence*

Japan

Yasuhiko Hori, *Chiba*
Hidetoshi Ikeda, *Koriyama*
Masahito Kawabori, *Sapporo*
Tamotsu Kamishima, *Sapporo*
Hiro Kiyosue, *Yufu*
Yasunori Minami, *Osaka-sayama*
Yasuhiro Morimoto, *Kitakyushu*
Satoru Murata, *Tokyo*
Shigeki Nagamachi, *Miyazaki*
Hiroshi Onishi, *Yamanashi*
Morio Sato, *Wakayama Shi*
Yoshito Tsushima, *Maebashi*
Masahiro Yanagawa, *Suita*

Netherlands

Willem Jan van Rooij, *Tilburg*

New Zealand

W Howell Round, *Hamilton*

Pakistan

Wazir Muhammad, *Abbottabad*

Poland

Maciej S Baglaj, *Wroclaw*

Piotr Czauderna, *Gdansk*

Portugal

Joao Manuel RS Tavares, *Porto*

Serbia

Olivera Ciraj-Bjelac, *Belgrade*

Singapore

Gopinathan Anil, *Singapore*
Terence KB Teo, *Singapore*
Cher Heng Tan, *Singapore*

Slovakia

Stefan Sivak, *Martin*

South Korea

Ki Seok Choo, *Busan*
Seung Hong Choi, *Seoul*
Dae-Seob Choi, *Jinju*
Hong-Seok Jang, *Seoul*
Yong Jeong, *Daejeon*
Chan Kyo Kim, *Seoul*
Se Hyung Kim, *Seoul*
Joong-Seok Kim, *Seoul*
Sang Eun Kim, *Seongnam*
Sung Joon Kwon, *Seoul*
Jeong Min Lee, *Seoul*
In Sook Lee, *Busan*
Noh Park, *Goyang*
Chang Min Park, *Seoul*
Sung Bin Park, *Seoul*
Deuk Jae Sung, *Seoul*
Choongsoo Shin, *Seoul*
Kwon-Ha Yoon, *Iksan*

Spain

Miguel A De Gregorio, *Zaragoza*
Antonio Luna, *Jaén*
Enrique Marco de Lucas, *Santander*
Fernando Ruiz Santiago, *Granada*

Sweden

Dmitry Grishenkov, *Stockholm*
Tie-Qiang Li, *Stockholm*

Switzerland

Nicolau Beckmann, *Basel*
Christian Boy, *Bern*
Giorgio Treglia, *Bellinzona*

Stephan Ulmer, *Kiel*

Thailand

Sirianong Namwongprom, *Chiang Mai*

Turkey

Kubilay Aydin, *Istanbul*
Ramazan Akdemir, *Sakarya*
Serhat Avcu, *Ankara*
Ayse Aralasmak, *Istanbul*
Oktay Algin, *Ankara*
Nevbahar Akcar, *Meselik*
Bilal Battal, *Ankara*
Zulkif Bozgeyik, *Elazig*
Nazan Ciledag, Aakara
Fuldem Y Donmez, *Ankara*
Gulgun Engin, *Istanbul*
Ahmet Y Goktay, *Izmir*
Oguzhan G Gumustas, *Bursa*
Kaan Gunduz, *Ankara*
Pelin Ozcan Kara, *Mersin*
Kivanc Kamburoglu, *Ankara*
Ozgur Kilickesmez, *Istanbul*
Furuzan Numan, *Istanbul*
Cem Onal, *Adana*
Ozgur Oztekin, *Izmir*
Seda Ozbek (Boruban), *Konya*
Selda Sarikaya, *Zonguldak*
Figen Taser, *Kutahya*
Baran Tokar, *Eskisehir*
Ender Uysal, *Istanbul*
Ensar Yekeler, *Istanbul*

United Kingdom

Indran Davagnanam, *London*
M DC Valdés Hernández, *Edinburgh*
Alan Jackson, *Manchester*
Suneil Jain, *Belfast*
Long R Jiao, *London*
Miltiadis Krokidis, *Cambridge*
Pradesh Kumar, *Liverpool*
Peter D Kuzmich, *Derby*
Georgios Plataniotis, *Brighton*
Vanessa Sluming, *Liverpool*

United States

Garima Agrawal, *Saint Louis*
James R Brasic, *Baltimore*
Rajendra D Badgaiyan, *Buffalo*
Ulas Bagci, *Bethesda*
Anat Biegon, *Stony Brook*
Ramon Casanova, *Winston Salem*
Wenli Cai, *Boston*
Zheng Chang, *Durham*
Corey J Chakarun, *Long Beach*
Kai Chen, *Los Angeles*
Hyun-Soon Chong, *Chicago*
Marco Cura, *Dallas*
Ravi R Desai, *Bensalem*
Delia DeBuc, *Miami*
Carlo N De Cecco, *Charleston*
Timm-Michael L Dickfeld, *Baltimore*
Subba R Digumarthy, *Boston*
Huy M Do, *Stanford*
Todd A Faasse, *Grand Rapids*
Salomao Faintuch, *Boston*
Girish M Fatterpekar, *New York*
Dhakshinamoorthy Ganeshan, *Houston*
Robert J Griffin, *Little Rock*
Andrew J Gunn, *Boston*
Sandeep S Hedgire, *Boston*
Timothy J Hoffman, *Columbia*
Mai-Lan Ho, *San Francisco*
Juebin Huang, *Jackson*
Abid Irshad, *Charleston*
Matilde Inglese, *New York*
El-Sayed H Ibrahim, *Jacksonville*
Paul R Julsrud, *Rochester*
Pamela T Johnson, *Baltimore*
Ming-Hung Kao, *Tempe*
Sunil Krishnan, *Houston*
Richard A Komoroski, *Cincinnati*
Sandi A Kwee, *Honolulu*
King Kim, *Ft. Lauderdale*
Guozheng Liu, *Worcester*
Yiyan Liu, *Newark*
Venkatesh Mani, *New York*
Lian-Sheng Ma, *Pleasanton*
Rachna Madan, *Boston*
Zeyad A Metwalli, *Houston*
Yilong Ma, *Manhasset*
Hui Mao, *Atlanta*
Feroze B Mohamed, *Philadelphia*
Gul Moonis, *Boston*
John L Nosher, *New Brunswick*
Rahmi Oklu, *Boston*
Aytekin Oto, *Chicago*
Bishnuhari Paudyal, *Philadelphia*
Rajul Pandya, *Youngstown*
Chong-Xian Pan, *Sacramento*
Jay J Pillai, *Baltimore*
Neal Prakash, *Duarte*
Reza Rahbar, *Boston*
Ali S Raja, *Boston*
Gustavo J Rodriguez, *El Paso*
David J Sahn, *Portlsand*
Steven Schild, *Scottsdale*
Ali R Sepahdari, *Los Angeles*
Li Shen, *Indianapolis*
JP Sheehan, *Charlottesville*
Atul B Shinagare, *Boston*
Sarabjeet Singh, *Boston*
Charles J Smith, *Columbia*
Kenji Suzuki, *Chicago*
Monvadi Srichai-Parsia, *Washington*
Sree H Tirumani, *Boston*
Hebert A Vargas, *New York*
Sachit Verma, *Philadelphia*
Yoichi Watanabe, *Minneapolis*
Li Wang, *Chapel Hill*
Carol C Wu, *Boston*
Shoujun Xu, *Houston*
Min Yao, *Cleveland*
Xiaofeng Yang, *Atlanta*
Qingbao Yu, *Albuquerque*
Aifeng Zhang, *Chicago*
Chao Zhou, *Bethlehem*
Hongming Zhuang, *Philadelphia*

WJR World Journal of Radiology

Contents

Monthly Volume 7 Number 8 August 28, 2015

EDITORIAL

184 Updates in advanced diffusion-weighted magnetic resonance imaging techniques in the evaluation of prostate cancer
Vargas HA, Lawrence EM, Mazaheri Y, Sala E

189 Lung cancer screening: Computed tomography or chest radiographs?
van Beek EJR, Mirsadraee S, Murchison JT

194 Magnetic resonance imaging-based interpretation of degenerative changes in the lower lumbar segments and therapeutic consequences
Maataoui A, Vogl TJ, Khan MF

198 Small bowel imaging of inflammatory bowel disease
Casciani E, De Vincentiis C, Gualdi GF

MINIREVIEWS

202 Imaging of bone metastasis: An update
O'Sullivan GJ, Carty FL, Cronin CG

ORIGINAL ARTICLE

Basic study

212 Development of biodegradable radiopaque microsphere for arterial embolization-a pig study
Liu YS, Lin XZ, Tsai HM, Tsai HW, Chen GC, Chen SF, Kang JW, Chou CM, Chen CY

World Journal of Radiology
Volume 7 Number 8 August 28, 2015

Contents

ABOUT COVER

Editorial Board Member of *World Journal of Radiology*, Kenji Suzuki, PhD, Assistant Professor, Department of Radiology, Division of the Biological Sciences, the University of Chicago, Chicago, IL 60637, United States

AIM AND SCOPE

World Journal of Radiology (*World J Radiol*, *WJR*, online ISSN 1949-8470, DOI: 10.4329) is a peer-reviewed open access academic journal that aims to guide clinical practice and improve diagnostic and therapeutic skills of clinicians.

WJR covers topics concerning diagnostic radiology, radiation oncology, radiologic physics, neuroradiology, nuclear radiology, pediatric radiology, vascular/interventional radiology, medical imaging achieved by various modalities and related methods analysis. The current columns of *WJR* include editorial, frontier, diagnostic advances, therapeutics advances, field of vision, mini-reviews, review, topic highlight, medical ethics, original articles, case report, clinical case conference (clinicopathological conference), and autobiography.

We encourage authors to submit their manuscripts to *WJR*. We will give priority to manuscripts that are supported by major national and international foundations and those that are of great basic and clinical significance.

INDEXING/ABSTRACTING

World Journal of Radiology is now indexed in PubMed Central, PubMed, Digital Object Identifier, and Directory of Open Access Journals.

FLYLEAF **I-III** Editorial Board

NAME OF JOURNAL
World Journal of Radiology

ISSN
ISSN 1949-8470 (online)

LAUNCH DATE
December 31, 2009

FREQUENCY
Monthly

EDITORIAL OFFICE
Jin-Lei Wang, Director
Xiu-Xia Song, Vice Director
World Journal of Radiology
Room 903, Building D, Ocean International Center,
No. 62 Dongsihuan Zhonglu, Chaoyang District,
Beijing 100025, China
Telephone: +86-10-59080039
Fax: +86-10-85381893
E-mail: editorialoffice@wjgnet.com
Help Desk: http://www.wjgnet.com/esps/helpdesk.aspx
http://www.wjgnet.com

PUBLISHER
Baishideng Publishing Group Inc
8226 Regency Drive,
Pleasanton, CA 94588, USA
Telephone: +1-925-223-8242
Fax: +1-925-223-8243
E-mail: bpgoffice@wjgnet.com
Help Desk: http://www.wjgnet.com/esps/helpdesk.aspx
http://www.wjgnet.com

PUBLICATION DATE
August 28, 2015

INSTRUCTIONS TO AUTHORS
Full instructions are available online at http://www.wjgnet.com/1949-8470/g_info_20100316162358.htm.

ONLINE SUBMISSION
http://www.wjgnet.com/esps/

World Journal of Radiology

Submit a Manuscript: http://www.wjgnet.com/esps/
Help Desk: http://www.wjgnet.com/esps/helpdesk.aspx
DOI: 10.4329/wjr.v7.i8.184

World J Radiol 2015 August 28; 7(8): 184-188
ISSN 1949-8470 (online)

EDITORIAL

Updates in advanced diffusion-weighted magnetic resonance imaging techniques in the evaluation of prostate cancer

Hebert Alberto Vargas, Edward Malnor Lawrence, Yousef Mazaheri, Evis Sala

Hebert Alberto Vargas, Edward Malnor Lawrence, Yousef Mazaheri, Evis Sala, Department of Radiology, Memorial Sloan Kettering Cancer Center, New York, NY 10065, United States

Author contributions: Vargas HA drafted the manuscript; all authors participated in the literature search, summary and interpretation; all authors edited and approved the final manuscript.

Conflict-of-interest statement: The authors have no conflicts of interest to disclose.

Correspondence to: Hebert Alberto Vargas, MD, Department of Radiology, Memorial Sloan Kettering Cancer Center, 1275 York Av., New York, NY 10065, United States. vargasah@mskcc.org
Telephone: +1-212-6392000

Received: February 28, 2015
Peer-review started: March 2, 2015
First decision: March 20, 2015
Revised: June 2, 2015
Accepted: June 18, 2015
Article in press: June 19, 2015
Published online: August 28, 2015

Abstract

Diffusion-weighted magnetic resonance imaging (DW-MRI) is considered part of the standard imaging protocol for the evaluation of patients with prostate cancer. It has been proven valuable as a functional tool for qualitative and quantitative analysis of prostate cancer beyond anatomical MRI sequences such as T2-weighted imaging. This review discusses ongoing controversies in DW-MRI acquisition, including the optimal number of b-values to be used for prostate DWI, and summarizes the current literature on the use of advanced DW-MRI techniques. These include intravoxel incoherent motion imaging, which better accounts for the non-mono-exponential behavior of the apparent diffusion coefficient as a function of b-value and the influence of perfusion at low b-values. Another technique is diffusion kurtosis imaging (DKI). Metrics from DKI reflect excess kurtosis of tissues, representing its deviation from Gaussian diffusion behavior. Preliminary results suggest that DKI findings may have more value than findings from conventional DW-MRI for the assessment of prostate cancer.

Key words: Prostate cancer; Diffusion-weighted imaging; Diffusion kurtosis imaging; Magnetic resonance imaging; Include intravoxel incoherent motion

Core tip: Diffusion-weighted magnetic resonance imaging (DW-MRI) is considered part of the standard imaging protocol for the evaluation of patients with prostate cancer. In this review we discuss the ongoing controversies in DW-MRI acquisition, including the optimal number of *b*-values to be used for prostate DWI, and summarize the current literature on the use of advanced DW-MRI techniques such as intravoxel incoherent motion imaging and diffusion kurtosis imaging.

Vargas HA, Lawrence EM, Mazaheri Y, Sala E. Updates in advanced diffusion-weighted magnetic resonance imaging

techniques in the evaluation of prostate cancer. *World J Radiol* 2015; 7(8): 184-188 Available from: URL: http://www.wjgnet.com/1949-8470/full/v7/i8/184.htm DOI: http://dx.doi.org/10.4329/wjr.v7.i8.184

INTRODUCTION

Diffusion-weighted (DW) techniques have been applied extensively for the evaluation of patients with prostate cancer and are now part of most standard prostate magnetic resonance imaging (MRI) clinical protocols. Multiple studies have demonstrated that DW-MRI contributes incremental value to T2-weighted MRI in the detection and localization of prostate cancer[1]. Straightforward, quantitative metrics from DW-MRI – most commonly apparent diffusion coefficient (ADC) values – have been used to distinguish between benign and malignant prostate tissue and also to evaluate prostate cancer aggressiveness[2]. ADC values have been found to correlate inversely with prostate cancer Gleason score as well as tumor proliferation markers such as Ki-67[2-4]. Nevertheless, ADC values of prostate cancer overlap substantially with those of normal prostate and benign conditions, such as prostatitis and post-biopsy inflammation. Therefore, advanced methods for DW-MRI acquisition, processing and interpretation are now being investigated with the goal of further strengthening the value of DW-MRI for prostate cancer assessment.

SELECTION OF *B*-VALUES FOR PROSTATE DW-MRI

The *b*-value is one of the main factors reflecting the strength of the diffusion effects in DW-MRI, with higher *b*-values representing stronger diffusion effects. There is as yet no consensus regarding the optimal choice of *b*-values for acquiring prostate DW-MRI. Absolute ADC values are highly dependent on the *b*-values selected and must therefore be applied cautiously, especially when attempting to define "cut-offs" for distinguishing particular conditions or disease states[5]. Higher *b*-values offer greater tumor-to-normal-tissue contrast but also decrease the signal-to-noise ratio. Tamada *et al*[6] evaluated 50 patients with prostate cancer undergoing 3T prostate DW-MRI acquired with *b*-values of 0, 1000 and 2000 s/mm^2; they found that lesion conspicuity and tumor-to-normal signal intensity ratio were higher when using *b*-values of 0 and 2000 s/mm^2 compared to those using *b*-values of 0 and 1000 s/mm^2[6]. There was a significant correlation between ADC values of tumor regions and Gleason scores at both *b*-values of 0 and 1000 s/mm^2 (rho = -0.602; $P < 0.001$) and 0 and 2000 s/mm^2 (rho = -0.645; $P < 0.001$)[6]. As an alternative to the acquisition of high-*b*-value images, some investigators have proposed "computing" them through voxelwise fitting from a set of images acquired at lower *b*-values. Using numerical simulations, Tamada *et al*[6] found that noise and the contrast-to-noise ratio were comparable between DW-MRI images that were "calculated" and those that were "acquired" at a *b*-value of 1400 s/mm^2 ($P = 0.395$). In one study, diagnostic performance of DW-MRI in prostate tumor detection was compared for four different combinations of measured and acquired *b*-values[7]. The AUCs for protocol A (T2-weighted images alone), B (T2-weighted images in combination with measured DW images with b 1000), C (T2-weighted images in combination with measured DW images with b 2000) and D (T2-weighted images in combination with computed DW images with b 2000) were 0.67, 0.80, 0.86 and 0.84, respectively[7]. Protocols C and D had significantly higher AUCs when compared to protocol B ($P < 0.05$)[7].

INTRAVOXEL INCOHERENT MOTION IMAGING

The optimal number of *b*-values for prostate DW-MRI also continues to be debated. A minimum of two *b*-values is required for monoexponential calculation of ADC. However, to better account for the non-mono-exponential behavior of the diffusion signal intensity at different *b*-values and the influence of perfusion at low *b*-values, intravoxel incoherent motion (IVIM), a model based on the use of three or more *b*-values, can be applied. The use of multiple *b*-values also reduces the influence of *b*-value selection on ADC measurements[8]. One study evaluated prostate DW-MRI acquired with four *b*-values (0, 50, 500, and 800 s/mm²) in 13 biopsy-proven prostate cancer patients and found that ADC (μm^2/ms), molecular diffusion coefficient (D, μm^2/ms) and perfusion fraction (f, %) were significantly lower ($P < 0.005$) in cancer (1.01 ± 0.22, 0.84 ± 0.19 and 14.27 ± 7.10% for ADC, D and f) than in benign tissue (1.49 ± 0.17, 1.21 ± 0.22 and 21.25% ± 8.32%, for ADC, D and f)[9]. Another study applied monoexponential and biexponential fits to diffusion decay curves obtained from 26 patients with prostate cancer using 10 *b*-values ranging from 10 to 1000 s/mm^2)[10]. In 81% of cases, biexponential functions were found to provide statistically better fits than monoexponential functions[10]. Biexponential IVIM was used to calculate the parameters D, f, and D*. Significantly lower values of ADC, D, and f were found in prostate cancer compared to the values in the normal prostatic peripheral zone (PZ), but similar values for f were reported in both benign hyperplastic changes and prostate cancer[10]. There were no significant differences between the D* values found in prostate cancer, benign hyperplasia, and PZ[10].

Some investigators have questioned whether IVIM truly contributes incremental value as compared to simple monoexponential ADC measurements in prostate cancer[11]. One study compared two different algorithms for generating IVIM metrics in 50 patients (27 known prostate cancer patients and 23 without

Table 1 Clinical studies of intravoxel incoherent motion imaging in prostate cancer

Ref.	No. of patients	Pathologic reference	*b*-values (s/mm^2)	MR parameters	PCa values[1]	Normal prostate values[1]	Significance
Döpfert *et al*[9]	13	TRUS biopsy	0, 50, 500, 800	3.0 T; TR/TE: 2600/66 ms; FOV: 204 mm × 204 mm; Matrix: 136 × 136; slice thickness: 3 mm; 8 averages	ADC: 1.01 ± 0.22 D: 0.84 ± 0.19 D*: 7.52 ± 4.77 f: 14.27 ± 7.10	ADC: 1.49 ± 0.17 D: 1.21 ± 0.22 D*: 6.82 ± 2.78 f: 21.25 ± 8.32	ADC, D, f significantly lower in PCa *vs* healthy prostate tissue Higher variation in maps of D and f compared to ADC
Shinmoto *et al*[10]	26	TRUS biopsy or RP	0, 10, 20, 30, 50, 80, 100, 200, 400, 1000	3.0 T; TR/TE: 5132/40 ms; Matrix: 80 × 80; slice thickness/gap: 3.5/0.1 mm; iPAT factor, 2; NEX = 2	ADC: 0.90 ± 0.16 D: 0.50 ± 0.15 D*: 5.35 ± 6.27 f: 35 ± 13	ADC: 1.76 ± 0.22 D: 0.89 ± 0.24 D*: 3.02 ± 0.86 f: 58 ± 11	ADC, D, f significantly lower in PCa *vs* noncancerous PZ Improved fit in 81% of study subjects for biexponential curve
Kuru *et al*[11]	27	MR-TRUS fusion biopsy	0, 50, 100, 150, 200, 250, 800	3.0 T; TR/TE: 3100/52 ms; FOV: 280 mm × 210 mm; Matrix: 128 × 96; slice thickness: 3 mm; iPAT factor, 2; 5 averages	ADC: 0.88 ± 0.29 D: 1.04 ± 0.23 D*: 31.1 ± 45.0 f: 9.5 ± 5.5	ADC: 1.56 ± 0.23 D: 1.44 ± 0.19 D*: 10.9 ± 4.0 f: 11.1 ± 5.0	Only D and ADC showed high AUC (≥ 0.90) for PCa *vs* normal Limited differentiation of PCa grade using f or D*
Pang *et al*[12]	33	MR-TRUS fusion biopsy	0, 188, 375, 563	3.0 T; TR/TE: 4584/59 ms; FOV:160 × 180 mm; slice thickness: 3.0 mm; iPAT factor, 2; 4+ averages	D: 0.99 ± 0.29 f: 7.2 ± 2.6 K^{trans}: 0.39 ±0.22 V_P: 8.4 ± 6.6	D: 1.76 ± 0.35 f: 3.7 ± 1 .9 K^{trans}: 0.18 ± 0.10 V_P: 3.4 ± 2.6	Significant increase in f for PCa *vs* normal prostate Pearson's correlation coefficient (r) for f and K^{trans} of 0.51

[1]Values are mean ± SD [ADC: Apparent diffusion coefficient (μm^2/ms); D: molecular diffusion coefficient (μm^2/ms); D*: Perfusion-related diffusion coefficient (μm^2/ms); f: Perfusion fraction (%); K^{trans}: Volume transfer constant (min^{-1}); V_P: Plasma fractional volume (%)]. AUC: Area under curve; FOV: Field of view; GS: Gleason score; iPAT: Integrated parallel acquisition techniques; IVIM: Intravoxel incoherent motion; MR: Magnetic resonance; NEX: Number of excitations; PCa: Prostate cancer; PZ: Peripheral zone; RP: Radical prostatectomy; T: Tesla; TE: Time of echo; TR: Time of repetition; TRUS: Transrectal ultrasound.

known cancer) who underwent prostate DWI acquired with 7 *b*-values (0, 50, 100, 150, 200, 250, and 800 s/mm^2)[11]. D was similar with the two algorithms (P = 0.22), but f was significantly different between the 2 (higher with algorithm 1) (P < 0.05). The AUCs for differentiating tumor and normal tissues were ⩾ 0.90 for D (from the 2 algorithms) and ADC (but not f or D*). IVIM-derived parameters are also influenced by the range of *b*-values used. Pang *et al*[12] analyzed prostate DW-MRI acquired with five *b*-values ranging between 188 and 750 s/mm^2) and assessed the influence of the choice of *b*-values on the measured D and f. Both parameters were markedly influenced by the choice of *b*-values. The best correlation with DCE-MRI was achieved when the IVIM parameters were calculated without the highest *b*-value (750 s/mm^2). Using this approach, significantly higher f from IVIM and ktrans and plasma fractional volume from DCE-MRI were found for prostate cancers (7.2%, 0.39/min and 8.4% respectively) compared to normal prostate tissue (3.7%, 0.18/min and 3.4% respectively)[12]. In summary, further research into prostate IVIM is needed, with a focus on selecting the most appropriate patient population and on standardizing image acquisition techniques and approaches to fit the IVIM parameters from the DW-MRI data. A summary of clinical studies of IVIM imaging in prostate cancer is presented in Table 1.

DIFFUSION KURTOSIS IMAGING IN PROSTATE CANCER

Diffusion kurtosis imaging (DKI) is another technique that has been used in attempts to more accurately characterize the multi-exponential behavior of diffusion decay in prostate cancer[13-18]. Metrics from DKI reflect excess kurtosis of the tissue, representing its deviation from Gaussian diffusion behavior[15]. Preliminary results suggest that DKI findings may have more value than findings from conventional DW-MRI for prostate cancer assessment.

In a study of 31 subjects (including healthy volunteers and patients undergoing evaluation for raised PSA levels), Quentin *et al*[14] performed DKI with 4 *b*-values ranging between 0 and 1000 s/mm^2 and with diffusion gradients applied in 20 different spatial directions; they found that there was a better fit to the diffusion weighted signal when using DKI compared to when using the monoexponential ADC[14]. Significantly higher mean (K_{mean}) and axial (K_{ax}) kurtosis were reported in prostate tumors (K_{mean} 1.84 ± 0.43; K_{ax} 1.78 ± 0.39,) compared to the normal PZ (K_{mean} 1.16 ± 0.13; K_{ax} 1.09 ± 0.12, P < 0.001) or the transition/central zone (K_{ax} 1.40 ± 0.12, K_{mean} 1.44 ± 0.17; P = 0.01, respectively)[14].

Another study of 47 patients with prostate cancer who underwent 3T DW-MRI using *b*-values up to 2000 s/mm^2 found that the DKI metric K, which represents non-Gaussian diffusion behavior, was significantly higher in prostate sextants involved by tumor compared to sextants containing non-cancerous prostate tissue (0.96 ± 0.24 *vs* 0.57 ± 0.07, P < 0.001) and was also significantly greater in Gleason score > 6 tumors (1.05 ± 0.26) compared to tumors with Gleason scores ⩽ 6 (0.89 ± 0.20; P < 0.001)[16]. For differentiating prostate sextants involved by cancer from non-cancerous prostate sextants, K showed significantly greater

Table 2 Clinical studies of diffusion kurtosis imaging in prostate cancer

Ref.	No. of patients	Pathologic reference	*b*-values (s/mm^2)	MR parameters	Quantitative parameters[1]	Significance
Quentin *et al*[14]	31	Biopsy	0, 300, 600, 1000	3.0 T; TR/TE: 1700/101 ms; FOV: 204 × 204 mm; Matrix: 136 × 136; slice thickness: 6 mm; iPAT factor, 2; 4 averages	K_{axial}, PCa: 1.78 ± 0.39 K_{axial}, TZ: 1.40 ± 0.12 K_{axial}, PZ: 1.09 ± 0.12	DKI better fit than monoexponential; Difference for K between PCa and normal TZ/PZ is significant
Rosenkrantz *et al*[16]	47	Biopsy	0, 500, 1000, 1500, 2000	3.0 T; TR/TE: 3500/81 ms; FOV: 280 mm × 218 mm; Matrix: 100 × 100; slice thickness: 4 mm; iPAT factor, 2; 6 averages	K, high GS: 1.05 ± 0.26 K, low GS: 0.89 ± 0.20 K, PZ: 0.57 ± 0.07	Significant difference between K in high GS *vs* low GS sextants; K found to have better sensitivity, AUC than ADC or D for PCa
Suo *et al*[17]	19	RP	0, 500, 800, 1200, 1500, 2000	3.0 T; TR/TE: 3940/106 ms; FOV: 280 mm × 280 mm; Matrix: 128 × 128; slice thickness/gap: 3/1 mm; 4 averages	K, PCa: 0.96 ± 0.20 K, PZ: 0.59 ± 0.08	Significant difference for K between PCa and normal PZ; GS correlates significantly with K
Tamura *et al*[18]	20	RP	0, 10, 20, 30, 50, 80, 100, 200, 400, 1000, 1500	3.0 T; TR/TE: 5000/49 ms; FOV: 240 × 240 mm; Matrix: 80 × 80; slice thickness/gap: 3.5/0.1 mm; iPAT factor, 2; NEX = 2	K, PCa: 1.19 ± 0.24 K, BPH: 0.99 ± 0.28 K, PZ: 0.63 ± 0.23	Significant difference for K between PCa and normal PZ but marked overlap for K between PCa and BPH

[1]Values are mean ± SD [K: Kurtosis parameter (unitless); K_{axial}: Axial kurtosis (unitless)]. AUC: Area under curve; BPH: Benign prostatic hyperplasia; DKI: Diffusional kurtosis imaging; FOV: Field of view; GS: Gleason score; iPAT: Integrated parallel acquisition techniques; MR: Magnetic resonance; NEX: Number of excitations; PCa: Prostate cancer; PZ: Peripheral zone; RP: Radical prostatectomy; T: Tesla; TE: Time of echo; TR: Time of repetition; TZ: Transitional zone.

sensitivity (0.93) than ADC (0.79) or the DKI parameter D (0.84; $P < 0.001$), which represents diffusion corrected for non-Gaussianity. There was no significant difference in specificity; $P > 0.99$)[16]. The sensitivity of K (0.69) was significantly greater than that of ADC (0.51) or D (0.49) for differentiating between low- and high-grade cancer sextants but the specificity was lower (0.70, 0.81 and 0.83 for K, ADC and D; $P \leqslant 0.023$)[16]. The AUC for differentiating prostate sextants with Gleason Score $\leqslant$ 6 tumors from those with Gleason Score > 6 tumors was greater for K (0.70) than ADC (0.62) ($P = 0.010$)[16]. Similar findings were reported in a study that evaluated 19 prostate patients undergoing DW-MRI[17]. ADC and D values were significantly lower and K values were significantly higher in cancerous compared to non-cancerous PZ (ADC= 0.79 mum^2/ms ± 0.14 *vs* 1.23 ± 0.19 mum^2/ms; D = 1.56 mum^2/ms ± 0.23 *vs* 2.54 ± 0.24 mum^2/ms; K 0.96 ± 0.20 *vs* 0.59 ± 0.08; $P < 0.001$ for all)[17]. In benign PZ and prostate cancer, D and K values overlapped less often than did ADC values[17]. A significant inverse correlation was observed between prostate cancer D and K values (Pearson correlation coefficient $r = -0.729$; $P < 0.001$)[17]. ADC and K values differed significantly in tumors with different Gleason scores ($P \leqslant 0.001$), however D values were similar across tumors with different Gleason scores ($P = 0.325$)[17]. Gleason score correlated significantly with both the ADC value ($r = -0.828$; $P < 0.001$) and the K ($r = 0.729$; $P < 0.001$).

Li *et al*[13] evaluated the utility of diffusion tensor imaging (DTI) and DCE-MRI for detecting prostate cancer of the PZ in 33 patients undergoing 3T MRI of the prostate before biopsy. DTI does not require the introduction of a diffusional kurtosis tensor in addition to the diffusion tensor used in DTI, and can be obtained with 2 b values. They found significant differences in the ADC, fractional anisotropy (FA), volume transfer constant (Ktrans), and rate constant (kep) values between prostate sextants containing prostate cancer *vs* prostate sextants containing benign PZ tissue ($P < 0.0001$ for all)[13]. For tumor detection, a significantly greater AUC was found for the combined DTI and DCE-MRI findings (0.93) compared to DTI (0.86,) or DCE-MRI (0.84) alone ($P = 0.0017$-0.0034)[13].

Despite the encouraging results obtained in the evaluation of prostate cancer with DKI and DTI, both alone and in combination with other MRI techniques, differentiating benign conditions such as prostatic hyperplasia from prostate cancer remains problematic. Tamura *et al*[18] performed DKI using 11 *b*-values (0-1500 s/mm^2) before radical prostatectomy in 20 patients and found DKI parameter K showed a trend toward higher levels in prostate cancer than in stromal benign prostatic hypertrophy, but there was marked overlap between the values in the 2 conditions (1.19 ± 0.24 *vs* 0.99 ± 0.28, $P = 0.051$)[13]. Further efforts to aid discrimination between benign (*e.g.*, inflammatory or hyperplastic) and malignant prostatic tissue are warranted.

DTI has also been applied in an effort to delineate the location and distribution of the periprostatic nerve fibers prior to prostatectomy, with the aim of improving nerve-sparing approaches. Panebianco *et al*[19] compared 2D and 3D T2-weighted images to DTI obtained with 16 gradient directions and $b = 0$ and 1000 s/mm^2 in 36 prostate cancer patients; reporting a partial ability to depict periprostatic nerve fibers using 2D and 3D T2 morphological sequences; with 3D-DTI allowing visualization in lal directions of the entire plexus of the periprostatic nerve fibers[19]. A summary of the clinical studies of DKI in prostate cancer is presented in Table 2.

CONCLUSION

Preliminary results suggest that IVIM , DKI and DTI may contribute incremental value to conventional DW-MRI for the detection of prostate cancer, the assessment of tumor aggressiveness, and the prediction of adverse final pathologic outcomes. However, IVIM DKI and DTI metrics have been found to overlap substantially between different prostate cancer grades as well as between cancer and benign conditions. While combining these techniques with other multiparametric MR sequences may further increase their usefulness, they are still in the early stages of development, and further research is needed to establish their roles in the evaluation of prostate cancer.

ACKNOWLEDGMENTS

We thank Mrs Ada Muellner, MS for editing this manuscript.

REFERENCES

1 **Tan CH**, Wei W, Johnson V, Kundra V. Diffusion-weighted MRI in the detection of prostate cancer: meta-analysis. *AJR Am J Roentgenol* 2012; **199**: 822-829 [PMID: 22997374 DOI: 10.2214/ajr.11.7805]

2 **Vargas HA**, Akin O, Franiel T, Mazaheri Y, Zheng J, Moskowitz C, Udo K, Eastham J, Hricak H. Diffusion-weighted endorectal MR imaging at 3 T for prostate cancer: tumor detection and assessment of aggressiveness. *Radiology* 2011; **259**: 775-784 [PMID: 21436085 DOI: 10.1148/radiol.11102066]

3 **Turkbey B**, Shah VP, Pang Y, Bernardo M, Xu S, Kruecker J, Locklin J, Baccala AA, Rastinehad AR, Merino MJ, Shih JH, Wood BJ, Pinto PA, Choyke PL. Is apparent diffusion coefficient associated with clinical risk scores for prostate cancers that are visible on 3-T MR images? *Radiology* 2011; **258**: 488-495 [PMID: 21177390 DOI: 10.1148/radiol.10100667]

4 **Zhang J**, Jing H, Han X, Huang Z, Cao Z, Liu Q. Diffusion-weighted imaging of prostate cancer on 3T MR: Relationship between apparent diffusion coefficient values and Ki-67 expression. *Acad Radiol* 2013; **20**: 1535-1541 [PMID: 24200480 DOI: 10.1016/j.acra.2013.09.007]

5 **Thörmer G**, Otto J, Reiss-Zimmermann M, Seiwerts M, Moche M, Garnov N, Franz T, Do M, Stolzenburg JU, Horn LC, Kahn T, Busse H. Diagnostic value of ADC in patients with prostate cancer: influence of the choice of b-values. *Eur Radiol* 2012; **22**: 1820-1828 [PMID: 22527373 DOI: 10.1007/s00330-012-2432-3]

6 **Tamada T**, Kanomata N, Sone T, Jo Y, Miyaji Y, Higashi H, Yamamoto A, Ito K. High b-value (2,000 s/mm2) diffusion-weighted magnetic resonance imaging in prostate cancer at 3 Tesla: comparison with 1,000 s/mm2 for tumor conspicuity and discrimination of aggressiveness. *PLoS One* 2014; **9**: e96619 [PMID: 24802652 DOI: 10.1371/journal.pone.0096619]

7 **Ueno Y**, Takahashi S, Kitajima K, Kimura T, Aoki I, Kawakami F, Miyake H, Ohno Y, Sugimura K. Computed diffusion-weighted imaging using 3-T magnetic resonance imaging for prostate cancer diagnosis. *Eur Radiol* 2013; **23**: 3509-3516 [PMID: 23881300 DOI: 10.1007/s00330-013-2958-z]

8 **Mazaheri Y**, Vargas HA, Akin O, Goldman DA, Hricak H. Reducing the influence of b-value selection on diffusion-weighted imaging of the prostate: evaluation of a revised monoexponential model within a clinical setting. *J Magn Reson Imaging* 2012; **35**: 660-668 [PMID: 22069141 DOI: 10.1002/jmri.22888]

9 **Döpfert J**, Lemke A, Weidner A, Schad LR. Investigation of prostate cancer using diffusion-weighted intravoxel incoherent motion imaging. *Magn Reson Imaging* 2011; **29**: 1053-1058 [PMID: 21855241 DOI: 10.1016/j.mri.2011.06.001]

10 **Shinmoto H**, Tamura C, Soga S, Shiomi E, Yoshihara N, Kaji T, Mulkern RV. An intravoxel incoherent motion diffusion-weighted imaging study of prostate cancer. *AJR Am J Roentgenol* 2012; **199**: W496-W500 [PMID: 22997399 DOI: 10.2214/ajr.11.8347]

11 **Kuru TH**, Roethke MC, Stieltjes B, Maier-Hein K, Schlemmer HP, Hadaschik BA, Fenchel M. Intravoxel incoherent motion (IVIM) diffusion imaging in prostate cancer - what does it add? *J Comput Assist Tomogr* 2014; **38**: 558-564 [PMID: 24733005 DOI: 10.1097/rct.0000000000000088]

12 **Pang Y**, Turkbey B, Bernardo M, Kruecker J, Kadoury S, Merino MJ, Wood BJ, Pinto PA, Choyke PL. Intravoxel incoherent motion MR imaging for prostate cancer: an evaluation of perfusion fraction and diffusion coefficient derived from different b-value combinations. *Magn Reson Med* 2013; **69**: 553-562 [PMID: 22488794 DOI: 10.1002/mrm.24277]

13 **Li C**, Chen M, Li S, Zhao X, Zhang C, Luo X, Zhou C. Detection of prostate cancer in peripheral zone: comparison of MR diffusion tensor imaging, quantitative dynamic contrast-enhanced MRI, and the two techniques combined at 3.0 T. *Acta Radiol* 2014; **55**: 239-247 [PMID: 23892233 DOI: 10.1177/0284185113494978]

14 **Quentin M**, Pentang G, Schimmöller L, Kott O, Müller-Lutz A, Blondin D, Arsov C, Hiester A, Rabenalt R, Wittsack HJ. Feasibility of diffusional kurtosis tensor imaging in prostate MRI for the assessment of prostate cancer: preliminary results. *Magn Reson Imaging* 2014; **32**: 880-885 [PMID: 24848289 DOI: 10.1016/j.mri.2014.04.005]

15 **Rosenkrantz AB**, Prabhu V, Sigmund EE, Babb JS, Deng FM, Taneja SS. Utility of diffusional kurtosis imaging as a marker of adverse pathologic outcomes among prostate cancer active surveillance candidates undergoing radical prostatectomy. *AJR Am J Roentgenol* 2013; **201**: 840-846 [PMID: 24059373 DOI: 10.2214/ajr.12.10397]

16 **Rosenkrantz AB**, Sigmund EE, Johnson G, Babb JS, Mussi TC, Melamed J, Taneja SS, Lee VS, Jensen JH. Prostate cancer: feasibility and preliminary experience of a diffusional kurtosis model for detection and assessment of aggressiveness of peripheral zone cancer. *Radiology* 2012; **264**: 126-135 [PMID: 22550312 DOI: 10.1148/radiol.12112290]

17 **Suo S**, Chen X, Wu L, Zhang X, Yao Q, Fan Y, Wang H, Xu J. Non-Gaussian water diffusion kurtosis imaging of prostate cancer. *Magn Reson Imaging* 2014; **32**: 421-427 [PMID: 24602826 DOI: 10.1016/j.mri.2014.01.015]

18 **Tamura C**, Shinmoto H, Soga S, Okamura T, Sato H, Okuaki T, Pang Y, Kosuda S, Kaji T. Diffusion kurtosis imaging study of prostate cancer: preliminary findings. *J Magn Reson Imaging* 2014; **40**: 723-729 [PMID: 24924835 DOI: 10.1002/jmri.24379]

19 **Panebianco V**, Barchetti F, Sciarra A, Marcantonio A, Zini C, Salciccia S, Collettini F, Gentile V, Hamm B, Catalano C. In vivo 3D neuroanatomical evaluation of periprostatic nerve plexus with 3T-MR Diffusion Tensor Imaging. *Eur J Radiol* 2013; **82**: 1677-1682 [PMID: 23773553 DOI: 10.1016/j.ejrad.2013.05.013]

P- Reviewer: Cai T, Ghatak S
S- Editor: Ji FF **L- Editor**: A **E- Editor**: Jiao XK

World Journal of Radiology

Submit a Manuscript: http://www.wjgnet.com/esps/
Help Desk: http://www.wjgnet.com/esps/helpdesk.aspx
DOI: 10.4329/wjr.v7.i8.189

World J Radiol 2015 August 28; 7(8): 189-193
ISSN 1949-8470 (online)

EDITORIAL

Lung cancer screening: Computed tomography or chest radiographs?

Edwin JR van Beek, Saeed Mirsadraee, John T Murchison

Edwin JR van Beek, Saeed Mirsadraee, Clinical Research Imaging Centre, Queen's Medical Research Institute, University of Edinburgh, Edinburgh EH16 4TJ, United Kingdom

Edwin JR van Beek, Saeed Mirsadraee, John T Murchison, Department of Radiology, Royal Infirmary of Edinburgh, Edinburgh EH16 4TJ, United Kingdom

Author contributions: The authors equally contributed to the literature research and editing of the manuscript; van Beek EJR was the guarantor for this work.

Conflict-of-interest statement: The authors have no conflicts of interest to declare.

Correspondence to: Edwin JR van Beek, MD, PhD, FRCR, FRCPE, Professor, Clinical Research Imaging Centre, Queen's Medical Research Institute, University of Edinburgh, CO.19, CRIC, QMRI, 47 Little France Crescent, Edinburgh EH16 4TJ, United Kingdom. edwin-vanbeek@ed.ac.uk
Telephone: +44-131-2427760
Fax: +44-131-2427773

Received: March 30, 2015
Peer-review started: April 4, 2015
First decision: April 27, 2015
Revised: April 29, 2015
Accepted: May 27, 2015
Article in press: May 28, 2015
Published online: August 28, 2015

Abstract

Worldwide, lung cancer is the leading cause of mortality due to malignancy. The vast majority of cases of lung cancer are smoking related and the most effective way of reducing lung cancer incidence and mortality is by smoking cessation. In the Western world, smoking cessation policies have met with limited success. The other major means of reducing lung cancer deaths is to diagnose cases at an earlier more treatable stage employing screening programmes using chest radiographs or low dose computed tomography. In many countries smoking is still on the increase, and the sheer scale of the problem limits the affordability of such screening programmes. This short review article will evaluate the current evidence and potential areas of research which may benefit policy making across the world.

Key words: Lung cancer; Chest radiograph; Computed tomography; Screening; Health economics

Core tip: The use of low dose computed tomography (CT) for lung cancer screening is superior to the use of standard chest radiograph (CXR), and therefore standard CXR should not be used for this purpose. However, the application of novel computer assisted diagnosis software may influence the utility of CXR and may ultimately be a cost-efficient method in those countries where delivery of low-dose CT is not feasible due to infrastructure or costs constraints.

van Beek EJR, Mirsadraee S, Murchison JT. Lung cancer screening: Computed tomography or chest radiographs? *World J Radiol* 2015; 7(8): 189-193 Available from: URL: http://www.wjgnet.com/1949-8470/full/v7/i8/189.htm DOI: http://dx.doi.org/10.4329/wjr.v7.i8.189

INTRODUCTION

Lung cancer is the most common cause of cancer

death in the United Kingdom accounting for 6% of overall national mortality and around 35000 deaths a year. In 2008 lung cancer was estimated to account for 18% of deaths world wide. Both one year and 5 years survival are inversely proportional to disease stage[1]. Current statistics in Scotland, which has a population of approximately 5.2 million, show an incidence of approximately 1 in 1000 with 8 in 10000 people dying due to lung cancer[2]. Similar incidence rates exist in other countries, and in the United States approximately 160000 deaths are due to lung cancer each year[3].

Most lung cancers are smoking related and smoking cessation is the most effective way of preventing this frequently fatal illness. The disease can be cured, especially if caught early. Stage 1, screening detected lung cancer has a 5-year survival rate in excess of 85%, whereas more advanced lung cancer invariably leads to death in less than 2 years[4]. As the lung cancer epidemic has grown and spread, ways of detecting the disease earlier, to improve the cure rate, have been explored. These have mainly been based around imaging using the chest radiograph (CXR) and computed tomography (CT).

CXR

In the early 1980s, a lung screening programme using 4-monthly CXRs in high risk patients was developed at the Mayo Clinic[5]. Subjects selected were over 45 years old male heavy smokers defined as one pack/day. They were randomly assigned to a control group (4593 patients) or repeated CXR follow up at 4 mo interval (4618 patients) after they had undergone an initial CXR and sputum cytology examination that were both normal. The follow up success was 75% at 4 mo, and 92 lung cancers were detected by CXR (of which 7 also had sputum cytology positive findings), while 15 patients had normal CXR with abnormal sputum cytology for an overall incidence of 109 (2.4%). A significant number of these lung cancers were visible in retrospect. Furthermore, 52 of the lung cancer were classified as stage Ⅰ (early disease; 35 of these were peripheral lesions), 4 were stage 2 disease (3 perihilar and 1 with hilar enlargement) while the 35 had stage 3 disease (15 peripheral lesions, 4 perihilar and 13 with hilar enlargement).

Another study in New York randomised a similar population of 10040 subjects to annual CXR only *vs* additional 4-monthly sputum cytology[6]. This study showed similar outcome between the two groups, with 288 detected lung cancers equally distributed between the two groups.

It was concluded from this study that the 4-monthly screening for lung cancer using chest radiography and sputum cytology, although capable of detecting up to 20% of lung cancers, was unable to improve mortality advantage over patients who were offered annual testing[7].

A more recent attempt at using CXR screening was carried out in the Prostate, Lung, Colorectal and Ovarian cancer screening trial[8]. This study randomised 154901 men and women aged 55-74 years to either standard care (77456) or annual screening (77445) for four years during the period 1993-2001. The number of lung cancer deaths was equal in both groups (1213 *vs* 1230) with similar stage and histology of lung cancers. Therefore, it was concluded that annual CXR screening does not benefit outcome of lung cancer mortality.

From these large scale studies, as well as from the National Lung Screening Trial (NLST) (see below), it is concluded that the application of routine annual chest radiography for screening of high-risk patients for lung cancer, although detecting a significant number of lung cancer cases, is not beneficial in terms of improvement of mortality.

CT

The NLST compared CXRs with computed tomography for the screening of patients at high risk for developing lung cancer[9]. Men and women were selected in the age group 55-74 years with a history of cigarette smoking of at least 30 pack years or had these exposure rates but had quit smoking within 15 years. The subjects were randomised to either three annual screening posterior-anterior CXRs (26732) or low-dose CT (26722). Almost 4-fold higher positive screening tests were obtained with CT (24.2% *vs* 6.9%), with the false positive rate slightly lower in the CXRs group (94.5% *vs* 96.4%). The incidence of proven lung cancer was higher in the CT group compared to the CXR group (relative risk 1.13; 95%CI: 1.03-1.23). More importantly, mortality due to lung cancer decreased from 309 deaths per 100000 person-years in the radiography group to 247 deaths from lung cancer per 100000 person-years in the low-dose CT group, a decrease of 20%. In addition, the CT group benefitted from other diagnoses that positively affected mortality rates, with 6.7% fewer patients dying in the low-dose CT group.

In Europe, several studies were started to evaluate the potential role of low-dose chest CT for lung cancer screening. Three studies did not demonstrate a benefit of lung cancer screening with CT in terms of mortality, but these were insufficiently powered to reliably draw such conclusion[10-12]. There are a further five ongoing studies that are yet to report on the final results, but some will be able to give answers to the question whether CT screening improves outcome of lung cancer patients[13-17].

The Nederlands-Leuvens Longkanker Screening Onderzoek (NELSON) study is a Dutch/Belgian project, which recruited 20000 high-risk subjects and randomised half of them for low-dose CT and the other half for CXR screening[13]. It is the largest European study and has sufficient power to enable a statement whether low-dose CT screening has benefit over chest radiography screening.

Another study from Canada has reported the first

screening round results and is focused on inclusion of cytology using autofluorescence bronchoscopy as well as modelling approaches towards optimisation of predictive value for lung nodules[18].

A potential risk associated with screening is the false positive results that can lead to further investigations and additional costs. A randomized, controlled trial of low-dose CT *vs* chest radiography (n = 3318 in both arms) as part of the NLST demonstrated a false-positive rate of 21% and 9% for single low-dose CT and chest radiography screening, respectively[19]. A total of 7% of participants with a false-positive low-dose CT examination and 4% with a false-positive chest radiography subsequently underwent an invasive procedure.

Another potential risk associate with lung cancer screening is the potential increased risk of lifetime cancers as a result of ionising radiation. The estimated risk of cancer from exposure to CT ionising radiation is reported to be more when the screening is started earlier in life, or on annual basis, and in females. A study reported an estimated 5.5% increase in lung cancer risk attributable to annual CT-related radiation exposure and concluded that a mortality benefit of considerably more than 5% may be necessary to outweigh the potential radiation risks[20].

Screening programs are associated with additional costs, both from the screening procedure and the follow up interventions. Previous studies reported that screening for lung cancer appeared to be cost-effective in high risk, more elderly populations[21,22]. Other studies questioned the potential cost effectiveness of lung cancer screening. However, their results were based on lower estimated effectiveness of screening than what was demonstrated by the NLST[23,24].

A more recent cost-utility analysis of lung cancer screening by low dose CT reported that repeat annual lung cancer screening in high risk adults aged 50-64 was highly cost-effective[25]. The study also indicated that offering smoking cessation interventions with the screening program improved the cost-effectiveness of lung cancer screening between 20%-45%.

A contrary report was published as part of a health technology assessment, which suggested that lung cancer screening would not be cost-effective[26]. However, it should be considered that this report was issued prior to the results of most of the recent large lung cancer screening trials.

The largest and most recent study, the NLST, also had an economic analysis and cost-effectiveness analysis performed[27]. This study demonstrated that the additional healthcare costs of performing low-dose CT screening would cost $1631 per person, with the incremental costs per life-year gained and the costs per quality adjusted life year gained coming in at $52000 and $81000, respectively. Importantly, there was quite a wide range of life year gains depending on age (optimal age range 60-69 years), risk for developing lung cancer (highest risk groups benefitting most) and gender (with women benefitting least). This caused a range of costs for quality adjusted life year gained anywhere between $32000-$615000. The study did not show a cost-effective benefit for chest radiography screening.

DISCUSSION

Clearly, based on the above studies, CT is superior to CXRs for screening in lung cancer. Although the NLST appears to have answered the question conclusively, there are still ongoing studies that may influence the manner in which screening will be approached in the future. Significant debate is still ongoing as to how often we should be screening, the optimal population that could benefit, interpretation of nodules, avoidance of false positive results and approaches including positron emission tomography-computed tomography, magnetic resonance imaging and autofluorescence bronchoscopy for instance[28-34]. Many of these points are still undergoing evaluation, and future study results are eagerly awaited.

There are some additional points to be taken into consideration, which may still give CXRs a potential role for screening of lung cancer.

First, CXRs have matured from a technical perspective, and the wide introduction of digital CXRs offers a new approach to application of computer assisted diagnosis (CAD). Thus, several studies have shown greater sensitivity for lung nodule detection using CAD methodologies, and this may be of benefit when using the test as a screening test[35,36]. However, a conclusive study showing the benefit of screening with chest radiography and added CAD has not been performed and could be important in this respect.

Second, CXRs are by far the cheaper of the two imaging modalities and more commonly available. This is an important issue, particularly in countries that are less well developed and where smoking continues to be on the increase and the lung cancer epidemic is on the rise. There is a high false negative rate using the CXR. CXR screening programmes should be backed up with cross-sectional imaging with a low threshold in place for investigating even small abnormalities detected on the CXR with CT scan. It may not be feasible to arrange for large-scale screening using CT and in these circumstances, one could consider using the CXR.

Whilst NLST demonstrated that benefits from early detection of lung cancer outweighs the risk of ionizing radiation, the potential risk is substantial. In NLST, participants received an average exposure of 8 mSv over 3 years of screening/diagnostic examinations which can potentially cause 1 cancer in every 2500 screened[37]. Recently, multiple studies have been investigating the feasibility of radiation dose reduction to sub-mSv level whilst the diagnostic accuracy is maintained[38,39]. Since there is a high contrast resolution between air and lung nodules, significant radiation dose reduction can be achieved while maintaining good diagnostic quality. Various strategies such as reduced

tube voltage, tube current, or both is being used. The application of iterative reconstruction would maintain spatial resolution in low dose studies whilst maintain diagnostic accuracy[40].

Overall, it is highly likely that low-dose CT screening for patients at high risk for developing lung cancer is a cost-effective approach which will lead to improved outcome due to earlier detection and treatment of this highly lethal malignancy. In countries that have the resources available, it makes sense therefore to use low-dose CT as a screening methodology. For countries where finances or logistics render low-dose CT screening impossible to deliver, CXRs on an annual basis should be considered and additional use of CAD may improve sensitivity for earlier lesions.

REFERENCES

1 **Cancer Research UK**. Lung cancer mortality statistics. [accessed 2013 May 11]. Available from: URL: http://www.cancerresearchuk.org/cancer-info/cancerstats/types/lung/mortality/uk-lung-cancer-mortality-statistics

2 **ISD Scotland**. Information and Statistics. Lung cancer and mesothelioma. [accessed 2013 August 7]. Available from: URL: http://www.isdscotland.org/Health-Topics/Cancer/Cancer-Statistics/Lung-Cancer-and-Mesothelioma/

3 **Siegel R**, Naishadham D, Jemal A. Cancer statistics, 2013. *CA Cancer J Clin* 2013; **63**: 11-30 [PMID: 23335087 DOI: 10.3322/caac.21166]

4 **Henschke CI**, Yankelevitz DF, Libby DM, Pasmantier MW, Smith JP, Miettinen OS. Survival of patients with stage I lung cancer detected on CT screening. *N Engl J Med* 2006; **355**: 1763-1771 [PMID: 17065637 DOI: 10.1056/NEJMoa060476]

5 **Muhm JR**, Miller WE, Fontana RS, Sanderson DR, Uhlenhopp MA. Lung cancer detected during a screening program using four-month chest radiographs. *Radiology* 1983; **148**: 609-615 [PMID: 6308709 DOI: 10.1148/radiology.148.3.6308709]

6 **Melamed MR**, Flehinger BJ, Zaman MB, Heelan RT, Perchick WA, Martini N. Screening for early lung cancer. Results of the Memorial Sloan-Kettering study in New York. *Chest* 1984; **86**: 44-53 [PMID: 6734291 DOI: 10.1378/chest.86.1.44]

7 **Fontana RS**, Sanderson DR, Woolner LB, Taylor WF, Miller WE, Muhm JR. Lung cancer screening: the Mayo program. *J Occup Med* 1986; **28**: 746-750 [PMID: 3528436]

8 **Oken MM**, Hocking WG, Kvale PA, Andriole GL, Buys SS, Church TR, Crawford ED, Fouad MN, Isaacs C, Reding DJ, Weissfeld JL, Yokochi LA, O'Brien B, Ragard LR, Rathmell JM, Riley TL, Wright P, Caparaso N, Hu P, Izmirlian G, Pinsky PF, Prorok PC, Kramer BS, Miller AB, Gohagan JK, Berg CD. Screening by chest radiograph and lung cancer mortality: the Prostate, Lung, Colorectal, and Ovarian (PLCO) randomized trial. *JAMA* 2011; **306**: 1865-1873 [PMID: 22031728 DOI: 10.1001/jama.2011.1591]

9 **Aberle DR**, Adams AM, Berg CD, Black WC, Clapp JD, Fagerstrom RM, Gareen IF, Gatsonis C, Marcus PM, Sicks JD. Reduced lung-cancer mortality with low-dose computed tomographic screening. *N Engl J Med* 2011; **365**: 395-409 [PMID: 21714641 DOI: 10.1056/NEJMoa1102873]

10 **Pedersen JH**, Ashraf H, Dirksen A, Bach K, Hansen H, Toennesen P, Thorsen H, Brodersen J, Skov BG, Døssing M, Mortensen J, Richter K, Clementsen P, Seersholm N. The Danish randomized lung cancer CT screening trial--overall design and results of the prevalence round. *J Thorac Oncol* 2009; **4**: 608-614 [PMID: 19357536 DOI: 10.1097/JTO.0b013e3181a0d98f]

11 **Infante M**, Cavuto S, Lutman FR, Brambilla G, Chiesa G, Ceresoli G, Passera E, Angeli E, Chiarenza M, Aranzulla G, Cariboni U, Errico V, Inzirillo F, Bottoni E, Voulaz E, Alloisio M, Destro A, Roncalli M, Santoro A, Ravasi G. A randomized study of lung cancer screening with spiral computed tomography: three-year results from the DANTE trial. *Am J Respir Crit Care Med* 2009; **180**: 445-453 [PMID: 19520905 DOI: 10.1164/rccm.200901-0076OC]

12 **Pastorino U**, Rossi M, Rosato V, Marchianò A, Sverzellati N, Morosi C, Fabbri A, Galeone C, Negri E, Sozzi G, Pelosi G, La Vecchia C. Annual or biennial CT screening versus observation in heavy smokers: 5-year results of the MILD trial. *Eur J Cancer Prev* 2012; **21**: 308-315 [PMID: 22465911 DOI: 10.1097/CEJ.0b013e328351e1b6]

13 **van Iersel CA**, de Koning HJ, Draisma G, Mali WP, Scholten ET, Nackaerts K, Prokop M, Habbema JD, Oudkerk M, van Klaveren RJ. Risk-based selection from the general population in a screening trial: selection criteria, recruitment and power for the Dutch-Belgian randomised lung cancer multi-slice CT screening trial (NELSON). *Int J Cancer* 2007; **120**: 868-874 [PMID: 17131307 DOI: 10.1002/ijc.22134]

14 **Blanchon T**, Bréchot JM, Grenier PA, Ferretti GR, Lemarié E, Milleron B, Chagué D, Laurent F, Martinet Y, Beigelman-Aubry C, Blanchon F, Revel MP, Friard S, Rémy-Jardin M, Vasile M, Santelmo N, Lecalier A, Lefébure P, Moro-Sibilot D, Breton JL, Carette MF, Brambilla C, Fournel F, Kieffer A, Frija G, Flahault A. Baseline results of the Depiscan study: a French randomized pilot trial of lung cancer screening comparing low dose CT scan (LDCT) and chest X-ray (CXR). *Lung Cancer* 2007; **58**: 50-58 [PMID: 17624475]

15 **Lopes Pegna A**, Picozzi G, Mascalchi M, Maria Carozzi F, Carrozzi L, Comin C, Spinelli C, Falaschi F, Grazzini M, Innocenti F, Ronchi C, Paci E. Design, recruitment and baseline results of the ITALUNG trial for lung cancer screening with low-dose CT. *Lung Cancer* 2009; **64**: 34-40 [PMID: 18723240 DOI: 10.1016/j.lungcan.2008.07.003]

16 **Becker N**, Motsch E, Gross ML, Eigentopf A, Heussel CP, Dienemann H, Schnabel PA, Pilz L, Eichinger M, Optazaite DE, Puderbach M, Tremper J, Delorme S. Randomized study on early detection of lung cancer with MSCT in Germany: study design and results of the first screening round. *J Cancer Res Clin Oncol* 2012; **138**: 1475-1486 [PMID: 22526165 DOI: 10.1007/s00432-012-1228-9]

17 **Baldwin DR**, Duffy SW, Wald NJ, Page R, Hansell DM, Field JK. UK Lung Screen (UKLS) nodule management protocol: modelling of a single screen randomised controlled trial of low-dose CT screening for lung cancer. *Thorax* 2011; **66**: 308-313 [PMID: 21317179]

18 **McWilliams A**, Tammemagi MC, Mayo JR, Roberts H, Liu G, Soghrati K, Yasufuku K, Martel S, Laberge F, Gingras M, Atkar-Khattra S, Berg CD, Evans K, Finley R, Yee J, English J, Nasute P, Goffin J, Puksa S, Stewart L, Tsai S, Johnston MR, Manos D, Nicholas G, Goss GD, Seely JM, Amjadi K, Tremblay A, Burrowes P, MacEachern P, Bhatia R, Tsao MS, Lam S. Probability of cancer in pulmonary nodules detected on first screening CT. *N Engl J Med* 2013; **369**: 910-919 [PMID: 24004118 DOI: 10.1056/NEJMoa1214726]

19 **Croswell JM**, Baker SG, Marcus PM, Clapp JD, Kramer BS. Cumulative incidence of false-positive test results in lung cancer screening: a randomized trial. *Ann Intern Med* 2010; **152**: 505-12, W176-80 [PMID: 20404381 DOI: 10.7326/0003-4819-152-8-201004200-00007]

20 **Brenner DJ**. Radiation risks potentially associated with low-dose CT screening of adult smokers for lung cancer. *Radiology* 2004; **231**: 440-445 [PMID: 15128988 DOI: 10.1148/radiol.2312030880]

21 **Henschke CI**, McCauley DI, Yankelevitz DF, Naidich DP, McGuinness G, Miettinen OS, Libby DM, Pasmantier MW, Koizumi J, Altorki NK, Smith JP. Early Lung Cancer Action Project: overall design and findings from baseline screening. *Lancet* 1999; **354**: 99-105 [PMID: 10408484 DOI: 10.1016/S0140-6736(99)06093-6]

22 **Marshall D**, Simpson KN, Earle CC, Chu CW. Economic decision analysis model of screening for lung cancer. *Eur J Cancer* 2001; **37**: 1759-1767 [PMID: 11549429 DOI: 10.1016/S0959-8049(01)0

0205-2]
23 **Mahadevia PJ**, Fleisher LA, Frick KD, Eng J, Goodman SN, Powe NR. Lung cancer screening with helical computed tomography in older adult smokers: a decision and cost-effectiveness analysis. *JAMA* 2003; **289**: 313-322 [PMID: 12525232 DOI: 10.1001/jama.289.3.313]
24 **Manser R**, Dalton A, Carter R, Byrnes G, Elwood M, Campbell DA. Cost-effectiveness analysis of screening for lung cancer with low dose spiral CT (computed tomography) in the Australian setting. *Lung Cancer* 2005; **48**: 171-185 [PMID: 15829317 DOI: 10.1016/j.lungcan.2004.11.001]
25 **Villanti AC**, Jiang Y, Abrams DB, Pyenson BS. A cost-utility analysis of lung cancer screening and the additional benefits of incorporating smoking cessation interventions. *PLoS One* 2013; **8**: e71379 [PMID: 23940744]
26 **Black C**, Bagust A, Boland A, Walker S, McLeod C, De Verteuil R, Ayres J, Bain L, Thomas S, Godden D, Waugh N. The clinical effectiveness and cost-effectiveness of computed tomography screening for lung cancer: systematic reviews. *Health Technol Assess* 2006; **10**: iii-iv, ix-x, 1-90 [PMID: 16409881]
27 **Black WC**, Gareen IF, Soneji SS, Sicks JD, Keeler EB, Aberle DR, Naeim A, Church TR, Silvestri GA, Gorelick J, Gatsonis C. Cost-effectiveness of CT screening in the National Lung Screening Trial. *N Engl J Med* 2014; **371**: 1793-1802 [PMID: 25372087 DOI: 10.1056/NEJMoa1312547]
28 **Field JK**, Oudkerk M, Pedersen JH, Duffy SW. Prospects for population screening and diagnosis of lung cancer. *Lancet* 2013; **382**: 732-741 [PMID: 23972816 DOI: 10.1016/S0140-6736(13)61614-1]
29 **Wood DE**. Maximizing the benefit and minimizing the risks of lung cancer screening. *J Thorac Imaging* 2012; **27**: 211-212 [PMID: 22695062 DOI: 10.1097/RTI.0b013e318256c22f]
30 **van Klaveren RJ**, Oudkerk M, Prokop M, Scholten ET, Nackaerts K, Vernhout R, van Iersel CA, van den Bergh KA, van 't Westeinde S, van der Aalst C, Thunnissen E, Xu DM, Wang Y, Zhao Y, Gietema HA, de Hoop BJ, Groen HJ, de Bock GH, van Ooijen P, Weenink C, Verschakelen J, Lammers JW, Timens W, Willebrand D, Vink A, Mali W, de Koning HJ. Management of lung nodules detected by volume CT scanning. *N Engl J Med* 2009; **361**: 2221-2229 [PMID: 19955524 DOI: 10.1056/NEJMoa0906085]
31 **Heuvelmans MA**, Oudkerk M, de Bock GH, de Koning HJ, Xie X, van Ooijen PM, Greuter MJ, de Jong PA, Groen HJ, Vliegenthart R. Optimisation of volume-doubling time cutoff for fast-growing lung nodules in CT lung cancer screening reduces false-positive referrals. *Eur Radiol* 2013; **23**: 1836-1845 [PMID: 23508275 DOI: 10.1007/s00330-013-2799-9]
32 **Pastorino U**, Bellomi M, Landoni C, De Fiori E, Arnaldi P, Picchio M, Pelosi G, Boyle P, Fazio F. Early lung-cancer detection with spiral CT and positron emission tomography in heavy smokers: 2-year results. *Lancet* 2003; **362**: 593-597 [PMID: 12944057 DOI: 10.1016/S0140-6736(03)14188-8]
33 **McWilliams AM**, Mayo JR, Ahn MI, MacDonald SL, Lam SC. Lung cancer screening using multi-slice thin-section computed tomography and autofluorescence bronchoscopy. *J Thorac Oncol* 2006; **1**: 61-68 [PMID: 17409828]
34 **Sommer G**, Tremper J, Koenigkam-Santos M, Delorme S, Becker N, Biederer J, Kauczor HU, Heussel CP, Schlemmer HP, Puderbach M. Lung nodule detection in a high-risk population: comparison of magnetic resonance imaging and low-dose computed tomography. *Eur J Radiol* 2014; **83**: 600-605 [PMID: 24364923 DOI: 10.1016/j.ejrad.2013.11.012]
35 **van Beek EJ**, Mullan B, Thompson B. Evaluation of a real-time interactive pulmonary nodule analysis system on chest digital radiographic images: a prospective study. *Acad Radiol* 2008; **15**: 571-575 [PMID: 18423313 DOI: 10.1016/j.acra.2008.01.018]
36 **White CS**, Flukinger T, Jeudy J, Chen JJ. Use of a computer-aided detection system to detect missed lung cancer at chest radiography. *Radiology* 2009; **252**: 273-281 [PMID: 19561261 DOI: 10.1148/radiol.2522081319]
37 **Bach PB**, Mirkin JN, Oliver TK, Azzoli CG, Berry DA, Brawley OW, Byers T, Colditz GA, Gould MK, Jett JR, Sabichi AL, Smith-Bindman R, Wood DE, Qaseem A, Detterbeck FC. Benefits and harms of CT screening for lung cancer: a systematic review. *JAMA* 2012; **307**: 2418-2429 [PMID: 22610500 DOI: 10.1001/jama.2012.5521]
38 **Mathieu KB**, Ai H, Fox PS, Godoy MC, Munden RF, de Groot PM, Pan T. Radiation dose reduction for CT lung cancer screening using ASIR and MBIR: a phantom study. *J Appl Clin Med Phys* 2014; **15**: 4515 [PMID: 24710436 DOI: 10.1120/jacmp.v15i2.4515]
39 **Tekath M**, Dutheil F, Bellini R, Roche A, Pereira B, Naughton G, Chamoux A, Michel JL. Comparison of the ultra-low-dose Veo algorithm with the gold standard filtered back projection for detecting pulmonary asbestos-related conditions: a clinical observational study. *BMJ Open* 2014; **4**: e004980 [PMID: 24879827 DOI: 10.1136/bmjopen-2014-004980]
40 **Rampinelli C**, Origgi D, Bellomi M. Low-dose CT: technique, reading methods and image interpretation. *Cancer Imaging* 2013; **12**: 548-556 [PMID: 23400217 DOI: 10.1102/1470-7330.2012.0049]

P- Reviewer: Hida T, Lassandro F, Pereira-Vega A, Yamaguchi K
S- Editor: Ji FF **L- Editor**: A **E- Editor**: Jiao XK

World Journal of Radiology

Submit a Manuscript: http://www.wjgnet.com/esps/
Help Desk: http://www.wjgnet.com/esps/helpdesk.aspx
DOI: 10.4329/wjr.v7.i8.194

World J Radiol 2015 August 28; 7(8): 194-197
ISSN 1949-8470 (online)

EDITORIAL

Magnetic resonance imaging-based interpretation of degenerative changes in the lower lumbar segments and therapeutic consequences

Adel Maataoui, Thomas J Vogl, M Fawad Khan

Adel Maataoui, Thomas J Vogl, M Fawad Khan, Institute for Diagnostic and Interventional Radiology, Goethe University, 60590 Frankfurt am Main, Germany

Author contributions: Maataoui A, Vogl TJ and Khan MF wrote the editorial and approved the version to be published.

Conflict-of-interest statement: The corresponding authors confirm that there are no conflicts of interest.

Correspondence to: Adel Maataoui, MD, Institute for Diagnostic and Interventional Radiology, Goethe University, Frankfurt, Theodor-Stern-Kai 7, 60590 Frankfurt am Main, Germany. adel.maataoui@gmx.de
Telephone: +49-69-63015534
Fax: +49-69-63014222

Received: January 29, 2015
Peer-review started: January 29, 2015
First decision: March 6, 2015
Revised: April 17, 2015
Accepted: May 16, 2015
Article in press: July 8, 2015
Published online: August 28, 2015

Abstract

Intervertebral disc degeneration and facet joint osteoarthritis of the lumbar spine are, among others, well known as a cause of low back and lower extremity pain. Together with their secondary disorders they set a big burden on health care systems and economics worldwide. Despite modern imaging modalities, such as magnetic resonance imaging, for a large proportion of patients with low back pain (LBP) it remains difficult to provide a specific diagnosis. The fact that nearly all the lumbar structures are possible sources of LBP, may serve as a possible explanation. Furthermore, our clinical experience confirms, that imaging alone is not a sufficient approach explaining LBP. Here, the Oswestry Disability Index, as the most commonly used measure to quantify disability for LBP, may serve as an easy-to-apply questionnaire to evaluate the patient's ability to cope with everyday life. For therapeutic purposes, among the different options, the lumbar facet joint intra-articular injection of corticosteroids in combination with an anaesthetic solution is one of the most frequently performed interventional procedures. Although widely used the clinical benefit of intra-articular steroid injections remains controversial. Therefore, prior to therapy, standardized diagnostic algorithms for an accurate assessment, classification and correlation of degenerative changes of the lumbar spine are needed.

Key words: Low back pain; Spine; Intervertebral disc disease; Facet joint osteoarthritis; Magnetic resonance imaging; Oswestry Disability Index

Core tip: Low back pain, caused by intervertebral disc degeneration (IDD) and facet joint osteoarthritis (FJOA), is a widely spread musculoskeletal disorder in all ages worldwide. Although IDD and FJOA are common findings on lumbar magnetic resonance-imaging, the relationship between imaging findings and clinical pain-presentation

as well as the benefit of different therapeutic options often remains unclear. This article briefly reviews the correlation of IDD and FJOA with clinical pain scores and discusses possible treatment options of FJOA with focus on the intra-articular injection of corticosteroids.

Maataoui A, Vogl TJ, Khan MF. Magnetic resonance imaging-based interpretation of degenerative changes in the lower lumbar segments and therapeutic consequences. *World J Radiol* 2015; 7(8): 194-197 Available from: URL: http://www.wjgnet.com/1949-8470/full/v7/i8/194.htm DOI: http://dx.doi.org/10.4329/wjr.v7.i8.194

INTRODUCTION

Among others, intervertebral disc degeneration (IDD) and facet joint osteoarthritis (FJOA) have been identified as causes for low back pain (LBP). Magnetic resonance imaging (MRI) is the imaging method of choice for the evaluation of IDD and FJOA of the lumbar spine[1,2]. For the grading of IDD of the lumbar spine Pfirrmann *et al*[3] proposed a MRI-based 5-point scale which is based on MRI signal intensity, disc structure, distinction between nucleus and annulus and disc height on T2-weighted, midsagittal images. Due to its more precise demonstration of bony details computed tomography (CT) often is the preferred modality in the evaluation of FJOA. Weishaupt *et al*[4] evaluated the significance of MRI in comparison to CT using an established 4-point scale. In summary, the authors conclude that an additional CT scan is not required in the presence of a MRI examination. Due to the fact that nearly all lumbar structures are possible sources of LBP, for a large proportion of patients it remains difficult to provide a specific diagnosis. The Oswestry Disability Index (ODI) is the most commonly used measure to quantify disability for LBP[5] and could reflect the relationship between pain and increasing grades of IDD and FJOA. If FJOA is identified as source of pain, multiple therapeutic options have been described and established[6]. Among the different options, the lumbar facet joint (LFJ) intra-articular injection of corticosteroids in combination with an anaesthetic solution is one of the most frequently performed interventional procedures[7]. The theory of this particular therapeutic approach is based on the idea that there is inflammation of the synovial structures of the degenerated facet joints. Thus intra-articular steroid injection is performed to generate an anti-inflammatory effect in order to achieve pain relief. Although widely used the clinical benefit of intra-articular steroid injections remains controversial[8]. The aim of the presented article is to highlight the relationship of increasing grades of IDD/FJOA and clinical pain scores and to discuss therapeutic success of minimally invasive therapeutic procedures, such as intra-articular steroid injections in degenerated facet joints.

SOURCES OF BACK PAIN

FJOA and pain correlation

Since the facet joints are the only synovial joints in the spine with hyaline cartilage overlying subchondral bone, a synovial membrane and a joint capsule, they develop degenerative changes that are equivalent to other peripheral joints. Different studies reported contradicting results about the prevalence of FJOA at lumbar levels. Kalichman *et al*[9] reported that FJOA is more prevalent at L4/5 (45.1%) followed by L5/S1 (38.2%) and L3/4 (30.6%) whereas Abbas *et al*[10] describe a different descending order: L5/S1 (55%), L4/5 (27%) and L3/4 (16%). Additionally, Abbas *et al*[10] describe that FJOA is an age dependant phenomenon, which increases cephalocaudally, whereas they found no correlation of FJOA with sex or the Body mass index. For the assessment of FJOA our group applied the 4-point scale as proposed by Weishaupt *et al*[4] on approximately 2400 facet joints of the lumbar segments L4/5 and L5/S1. Assuming that grade Ⅰ changes already represent mild degenerative changes, nearly all patients in our study group showed degenerative alterations of the facet joints (97% L4/5; 98% L5/S1). In 150 patients Ashraf *et al*[11] classified degenerative changes of the lumbar spine on lateral radiographs according to the criteria of Kellgren and Lawrence. Additionally, functional disability was measured using the ODI. They found no significant correlation between the morphological severity of osteoarthritis and ODI scores. Peterson *et al*[12] evaluated 172 consecutive patients with LBP. Lumbar radiographs were judged with regard to the severity of disc and facet joint degeneration. Results were correlated with the data of the ODI. The authors describe a weak correlation between the values of LBP and radiologically assessed lumbar spine degeneration. A major limitation of the mentioned studies is the fact that degenerative changes of the cervical and lumbar spine were graded on plain film radiographs, which are because of superposition of limited diagnostic value. Additionally, severity of degeneration of intervertebral discs as well as of facet joints was taken into account for scoring. As already mentioned nearly all-lumbar structures are possible sources of LBP, so that an isolated contemplation of anatomic structures (facet joint, intervertebral disc) and their degenerative changes with regard to clinical importance is necessary. Therefore we correlated degenerative changes of facet joints at lumbar levels L4/5 and L5/S1 with the ODI. Our results demonstrate that there is only a weak correlation between signs of degeneration and clinical disability scores as evaluated by ODI. Taking into account that a huge majority of patients of all ages show degenerative changes of facet joints in the lower motion segments of the lumbar spine, these results should be considered in the future evaluation of lumbar MRIs. In the presence of other degenerative changes like IDD, osteochondrosis or Morbus Baastrup the finding of FJOA shouldn't be

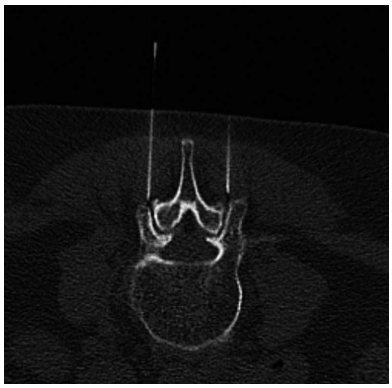

Figure 1 Computed tomography-guided puncture of the facet joints at lumbar levels L4/5 showing the needle trajectory.

considered evidentiary as the cause of LBP. In fact, the presented results seem to prove that chronic LBP is a multifactorial disorder, which cannot be explained with a constricted view on one lumbar compartment.

IDD and pain correlation

It is widely accepted that IDD of the lumbar spine is one of the main cause of lower back pain[13,14]. The etiology of IDD is not fully explained - heavy physical loading[15], overweight[16,17], vibrations during vehicle driving[18] and smoking[19] have been suggested to be associated with IDD. Since radiological features of IDD are almost universal in adults, it often remains unclear to what extent these changes are responsible for the clinical symptoms of the patient. From the radiological point of view, in the first place a standardized nomenclature in the evaluation of intervertebral disc alterations is needed. Pfirrmann *et al*[3] proposed a morphologic grading system which is based on MRI T2-weighted sagittal imaging and showed a good intra- and interobserver reliability. The grading system reflects the loss of proteoglycan concentration[20] in the nucleus pulposus of the lumbar disc, which goes along with a decreasing signal intensity in T2-weighted imaging. The experience of our group confirms the fact that IDD is a general finding in MRI of the lower (L4/5 and L5/S1) lumbar segments even in young-aged patients. The vast majority of examined patients presents with Pfirrmann grade Ⅱ - grade Ⅳ changes, whereas a relatively low percentage of lumbar discs present with grade Ⅴ changes. Only a small number of lumbar discs show no degenerative changes. These experiences impressively illustrate the dilemma to rate the clinical symptoms of the patient correctly, based on a pervasive imaging finding. In consensus to the above mentioned results regarding the correlation of FJOA and ODI scores, also the presence of IDD in lumbar MRI can't be considered evidentiary as a reason for LBP.

LFJ intra-articular steroid injections

LFJ intra-articular injections of corticosteroids in combination with an anaesthetic solution is one of the most frequently performed interventional procedures worldwide[7]. The theory of this particular therapeutic approach is based on the idea that there is inflammation of the synovial structures of the degenerated facet joints. Thus intra-articular steroid injection is performed to generate an anti-inflammatory effect in order to achieve pain relief. Although widely used the clinical benefit of intra-articular steroid injections remains controversial[8]. Lakemeier *et al*[21] compared the effectiveness of intra-articular steroid injections and radiofrequency denervation in relief of LBP associated with L3/L4 - L5/S1 FJOA[21]. They investigated the therapeutic effect of aforementioned interventional procedures in a cohort of 56 patients randomized in two therapeutic groups. In their double-blinded study the authors found no significant differences in the therapeutic success between the two procedures over a follow-up period of 6 mo. Ribeiro *et al*[22] compared the therapeutic success of intra-articular steroid injection *vs* intramuscular steroid application in patients with facet joint- related CLP. The experimental group received bilateral intra-articular steroid injection of segments L3/4 - L5/S1 (in total 6 injections), while the control group received 6 intramuscular injections on bilateral surface points of the paravertebral lumbar musculature. Both treatments were effective over the follow-up period of 6 mo compared to the baseline. Regarding pain - relief no significant difference between the procedures was observed. It is well known that besides technical modifications many additional factors are involved in therapeutic outcome. Gryll *et al*[23] reported about situational factors contributing to placebo effect during oral surgery (status of communicator of drug effects, attitude of dentist, attitude of dental technician and message of drug effects). Among the four variables only the attitude of the dentist and the dental technician led to a statistically significantly reduced fear of injection and lower ratings of pain experience from mandibular-block injection. Initial results of our group show, that the therapist's attitude and empathy may increase the therapeutic effect of LFJ intra-articular steroid injections in patients suffering from chronic LBP. Therefore, we performed a CT-guided puncture (Figure 1) of the facet joints at lumbar levels L4/5 or L5/S1, followed by an injection of a mixture of 4 mL of 0.5% bupivacaine and 1 mL of triamcinolone acetate (20 mg). After the therapeutic procedure we encouraged the patients of an experimental group to ask questions about the procedure and showed them representative CT-images. Patients of the control group left the interventional unit without further contact with the interventional radiologist. The initial results show a significant effect on pain relief during the early post-interventional phase in the experimental group as compared to the control group. It seems that in patients who better understand therapies applied on them, an increase in therapeutic efficacy can be observed. Explanatory behind the higher efficacy might be the phenomenon of hetero-suggestion, which occurs during the post-interventional patient-radiologist dialog during image presentation and might be conveying a message into the subconscious[24]. This shows how the open and transparent handling can lead to a strong therapeutic alliance between patients and physicians for the benefit of patients.

CONCLUSION

Age-dependent IDD and FJOA of the lumbar spine is reliably detected by MRI. The lack of significant correlation of IDD and FJOA with clinical pain scores such as the ODI confirms our experience that imaging alone is an insufficient approach explaining LBP. Clinical correlation is not an adjunct only but imperative for an adequate clinical approach in patients with LBP and lower extremity pain. Thus further studies are needed to correlate imaging data and clinical scores such as the Ostwestry disablility index. Among the different options for the treatment of LFJ-associated LBP, the intra-articular injection of corticosteroids and anaesthetic solutions is one of the most frequently performed procedures. Beside technical modifications it seems that patients who better understand therapies applied on them experience an increased therapeutic efficacy. This could be helpful in the daily clinical routine, where psychological phenomena such as hetero-suggestion can be used as a powerful and easy-to-apply tool, to support therapeutic procedures such as intra-articular injections.

REFERENCES

1 **Emch TM**, Modic MT. Imaging of lumbar degenerative disk disease: history and current state. *Skeletal Radiol* 2011; **40**: 1175-1189 [PMID: 21847748 DOI: 10.1007/s00256-011-1163-x]

2 **Sasiadek MJ**, Bladowska J. Imaging of degenerative spine disease--the state of the art. *Adv Clin Exp Med* 2012; **21**: 133-142 [PMID: 23214277]

3 **Pfirrmann CW**, Metzdorf A, Zanetti M, Hodler J, Boos N. Magnetic resonance classification of lumbar intervertebral disc degeneration. *Spine* (Phila Pa 1976) 2001; **26**: 1873-1878 [PMID: 11568697 DOI: 10.1097/00007632-200109010-00011]

4 **Weishaupt D**, Zanetti M, Boos N, Hodler J. MR imaging and CT in osteoarthritis of the lumbar facet joints. *Skeletal Radiol* 1999; **28**: 215-219 [PMID: 10384992 DOI: 10.1007/s002560050503]

5 **Fairbank JC**, Couper J, Davies JB, O'Brien JP. The Oswestry low back pain disability questionnaire. *Physiotherapy* 1980; **66**: 271-273 [PMID: 6450426]

6 **Cohen SP**, Huang JH, Brummett C. Facet joint pain--advances in patient selection and treatment. *Nat Rev Rheumatol* 2013; **9**: 101-116 [PMID: 23165358 DOI: 10.1038/nrrheum.2012.198]

7 **Manchikanti L**, Pampati V, Singh V, Falco FJ. Assessment of the escalating growth of facet joint interventions in the medicare population in the United States from 2000 to 2011. *Pain Physician* 2013; **16**: E365-E378 [PMID: 23877460]

8 **Manchikanti L**, Datta S, Gupta S, Munglani R, Bryce DA, Ward SP, Benyamin RM, Sharma ML, Helm S, Fellows B, Hirsch JA. A critical review of the American Pain Society clinical practice guidelines for interventional techniques: part 2. Therapeutic interventions. *Pain Physician* 2010; **13**: E215-E264 [PMID: 20648212]

9 **Kalichman L**, Li L, Kim DH, Guermazi A, Berkin V, O'Donnell CJ, Hoffmann U, Cole R, Hunter DJ. Facet joint osteoarthritis and low back pain in the community-based population. *Spine* (Phila Pa 1976) 2008; **33**: 2560-2565 [PMID: 18923337 DOI: 10.1097/BRS.0b013e318184ef95]

10 **Abbas J**, Hamoud K, Peleg S, May H, Masharawi Y, Cohen H, Peled N, Hershkovitz I. Facet joints arthrosis in normal and stenotic lumbar spines. *Spine* (Phila Pa 1976) 2011; **36**: E1541-E1546 [PMID: 21270684 DOI: 10.1097/BRS.0b013e318210c889]

11 **Ashraf A**, Farahangiz S, Pakniat Jahromi B, Setayeshpour N, Naseri M, Nasseri A. Correlation between Radiologic Sign of Lumbar Lordosis and Functional Status in Patients with Chronic Mechanical Low Back Pain. *Asian Spine J* 2014; **8**: 565-570 [PMID: 25346808 DOI: 10.4184/asj.2014.8.5.565]

12 **Peterson CK**, Bolton JE, Wood AR. A cross-sectional study correlating lumbar spine degeneration with disability and pain. *Spine* (Phila Pa 1976) 2000; **25**: 218-223 [PMID: 10685487 DOI: 10.1097/00007632-200001150-00013]

13 **Cheung KM**, Samartzis D, Karppinen J, Luk KD. Are "patterns" of lumbar disc degeneration associated with low back pain?: new insights based on skipped level disc pathology. *Spine* (Phila Pa 1976) 2012; **37**: E430-E438 [PMID: 22466575 DOI: 10.1097/BRS.0b013e3182304dfc]

14 **Takatalo J**, Karppinen J, Niinimäki J, Taimela S, Näyhä S, Mutanen P, Sequeiros RB, Kyllönen E, Tervonen O. Does lumbar disc degeneration on magnetic resonance imaging associate with low back symptom severity in young Finnish adults? *Spine* (Phila Pa 1976) 2011; **36**: 2180-2189 [PMID: 21358475 DOI: 10.1097/BRS.0b013e3182077122]

15 **Hangai M**, Kaneoka K, Kuno S, Hinotsu S, Sakane M, Mamizuka N, Sakai S, Ochiai N. Factors associated with lumbar intervertebral disc degeneration in the elderly. *Spine J* 2008; **8**: 732-740 [PMID: 18037353 DOI: 10.1016/j.spinee.2007.07.392]

16 **Samartzis D**, Karppinen J, Chan D, Luk KD, Cheung KM. The association of lumbar intervertebral disc degeneration on magnetic resonance imaging with body mass index in overweight and obese adults: a population-based study. *Arthritis Rheum* 2012; **64**: 1488-1496 [PMID: 22287295 DOI: 10.1002/art.33462]

17 **Takatalo J**, Karppinen J, Taimela S, Niinimäki J, Laitinen J, Sequeiros RB, Samartzis D, Korpelainen R, Näyhä S, Remes J, Tervonen O. Association of abdominal obesity with lumbar disc degeneration--a magnetic resonance imaging study. *PLoS One* 2013; **8**: e56244 [PMID: 23418543 DOI: 10.1371/journal.pone.0056244]

18 **Luoma K**, Riihimäki H, Raininko R, Luukkonen R, Lamminen A, Viikari-Juntura E. Lumbar disc degeneration in relation to occupation. *Scand J Work Environ Health* 1998; **24**: 358-366 [PMID: 9869307 DOI: 10.5271/sjweh.356]

19 **Wahlström J**, Burström L, Nilsson T, Järvholm B. Risk factors for hospitalization due to lumbar disc disease. *Spine* (Phila Pa 1976) 2012; **37**: 1334-1339 [PMID: 22281487 DOI: 10.1097/BRS.0b013e31824b5464]

20 **Pearce RH**, Thompson JP, Bebault GM, Flak B. Magnetic resonance imaging reflects the chemical changes of aging degeneration in the human intervertebral disk. *J Rheumatol Suppl* 1991; **27**: 42-43 [PMID: 2027127]

21 **Lakemeier S**, Lind M, Schultz W, Fuchs-Winkelmann S, Timmesfeld N, Foelsch C, Peterlein CD. A comparison of intraarticular lumbar facet joint steroid injections and lumbar facet joint radiofrequency denervation in the treatment of low back pain: a randomized, controlled, double-blind trial. *Anesth Analg* 2013; **117**: 228-235 [PMID: 23632051 DOI: 10.1016/j.spinee.2013.10.007]

22 **Ribeiro LH**, Furtado RN, Konai MS, Andreo AB, Rosenfeld A, Natour J. Effect of facet joint injection versus systemic steroids in low back pain: a randomized controlled trial. *Spine* (Phila Pa 1976) 2013; **38**: 1995-2002 [PMID: 23921331 DOI: 10.1097/BRS.0b013e3182a76df1]

23 **Gryll SL**, Katahn M. Situational factors contributing to the placebos effect. *Psychopharmacology* (Berl) 1978; **57**: 253-261 [PMID: 97705 DOI: 10.1007/bf00426747]

24 **Mommaerts JL**, Devroey D. The placebo effect: how the subconscious fits in. *Perspect Biol Med* 2012; **55**: 43-58 [PMID: 22643715 DOI: 10.1353/pbm.2012.0005]

P- Reviewer: Kara PO, Kilickesmez O
S- Editor: Tian YL **L- Editor**: A **E- Editor**: Jiao XK

World Journal of Radiology

Submit a Manuscript: http://www.wjgnet.com/esps/
Help Desk: http://www.wjgnet.com/esps/helpdesk.aspx
DOI: 10.4329/wjr.v7.i8.198

World J Radiol 2015 August 28; 7(8): 198-201
ISSN 1949-8470 (online)

EDITORIAL

Small bowel imaging of inflammatory bowel disease

Emanuele Casciani, Chiara De Vincentiis, Gianfranco Gualdi

Emanuele Casciani, Gianfranco Gualdi, Department of Emergency Radiology, "La Sapienza" University-Hospital Umberto I, 00166 Rome, Italy

Chiara De Vincentiis, Department of Radiology, "La Sapienza" University-Sant'Andrea's Hospital, 00189 Rome, Italy

Author contributions: Casciani E designed the study and wrote the manuscript; De Vincentiis C acquired the material, analysed data and helped to write the manuscript; Gualdi GF provided the collection of part of the material.

Conflict-of-interest statement: We have read and understood BPG's revision policy on declaration of interests and declare that we have no competing interests.

Correspondence to: Dr. Emanuele Casciani, Department of Emergency Radiology, "La Sapienza" University-Hospital Umberto I, Viale del Policlinico 155, 00166 Rome, Italy. emanuelecasciani@gmail.com
Telephone: +39-6-49979465
Fax: +39-6-6630218

Received: January 28, 2015
Peer-review started: February 1, 2015
First decision: March 6, 2015
Revised: March 26, 2015
Accepted: May 26, 2015
Article in press: May 27, 2015
Published online: August 28, 2015

Abstract

The study of the small bowel (SB) has always been challenging both for clinicians and radiologist. It is a long and tortuous tube that can be affected by various pathologies whose signs and symptoms are usually non specific and can mimic other acute abdominal disorders. For these reasons, imaging plays a central role in the diagnosis of the different pathological conditions that can occur. They are important also in the management and follow up of chronic diseases. We expose and evaluate all the radiological methods that are now available for the study of the SB with particular emphasis on the technological improvement of cross-sectional imaging, such as computed tomography (CT) and magnetic resonance imaging (MRI). These techniques have, infact, highly improved in terms of execution times (fast acquisitions images), patients discomfort and radiation dose, for CT, with consequent reduced biological risks. Moreover, the new post-processing options with multiplanar reconstruction and isotropic images have made significant changes in the evaluation of the exams. Especially MRI scans have been improved by the advent of new sequences, such as diffusion weighted imaging and cine-MRI, parallel imaging and breath-hold sequences and can provide excellent soft-tissue contrast without the use of ionizing radiations.

Key words: Small bowel imaging; Magnetic resonance; Cross-sectional imaging; Computed tomography; Positron emission tomography-computed tomography

Core tip: The small bowel (SB) has always been a challenging organ for clinical and radiologic evaluation. The purpose of our article is to evaluate all the imaging methods now available for the study of the SB with particular emphasis on the technological improvement of cross-sectional imaging.

Casciani E, De Vincentiis C, Gualdi GF. Small bowel imaging of inflammatory bowel disease. *World J Radiol* 2015; 7(8): 198-201

Available from: URL: http://www.wjgnet.com/1949-8470/full/v7/i8/198.htm DOI: http://dx.doi.org/10.4329/wjr.v7.i8.198

INTRODUCTION

Radiological studies of the small bowel were firstly performed at the beginning of this century by Morse and Cole[1] in 1927 and Pesquera[2] in 1929. From then until the early 2000s, barium contrast studies have been the only imaging methods to study the small bowel. In the last decade, a tremendous technological improvement of cross-sectional imaging [Ultrasound (US), computed tomography (CT), and magnetic resonance imaging (MRI)] have occurred. US scanners have significantly improved, now allowing a good visualization of the small bowel loops. Both CT and MRI scanners have become very fast (short execution times and less discomfort for the patients) and can create multiplanar reconstruction and isotropic images, the former with less radiation dose and the latter in the lack of ionizing radiations, particularly important in young patients who need periodic imaging examinations. Especially MRI scans have been improved by the advent of new sequences, such as diffusion weighted (DWI) and cine-MRI, parallel imaging and breath-hold sequences and can provide excellent soft-tissue contrast.

A complete exam requires the use of both intravenous and endoluminal contrast. The latter is necessary to obtain a good distension of the bowel loops and can be administered orally (MRI-Enterography) or through a nasojejunal tube (MRI-Enteroclysis). The MRI-Enterography is more comfortable for the patient but the MRI-Enteroclysis provides a better bowel distension, especially of the proximal loops, and, for this reason, is always the method of choice in patients with suspected jejunal lesions or recurrent intestinal subocclusion. Finally, since 2001, wireless capsule endoscopy has been introduced as another non-invasive technique for the evaluation of the entire small bowel, in which traditional endoscopy had severe limits[3]. Despite the important diagnostic innovation, the impossibility to perform therapeutic interventions is a high limit and, for this reason new endoscopic method were proposed in the subsequent years, such as Double-balloon endoscopy, in 2003, Single-balloon enteroscopy in 2007 and spiral enteroscopy in 2008[3].

Alternatively, also scintigraphy and positron emission tomography/computed tomography (PET/CT) has been reported, in several studies[4-6], as valid and non-invasive method to diagnose and assess disease activity in IBD. Regarding Scintigraphy, various biomarkers of inflammation, used to label white blood cells, such as technetium-99m hexamethylpropylene amine oxime (Tc-99m HMPAO WBC), pentavalent Tc-99m dimercaptosuccinic acid [Tc-99m (V) DMSA] and fluorine-18 fluorodeoxyglucose (18F-FDG), are widely accepted as accurate for the diagnosis of IBD[4]. Studies on ^{18}F-FDG PET/CT showed a significant correlation between the ^{18}F-FDG uptake PET-CT and the Crohn's disease endoscopy index of severity especially in segments with moderate to severe lesions. Moreover, ^{18}F-FDG PET may potentially provide information on the dynamic inflammatory changes occurring in inflammatory bowel disease (IBD), particularly Crohn's disease, being useful not only in the diagnosis but also in the follow up of the disease[5,6].

Thanks to these technical improvements in imaging, the cross-sectional techniques are replacing barium exams in the study of the small intestine, especially in IBD, both in adult and pediatric patients.

The "Porto criteria" recommend small-bowel follow-through (SBFT) as the imaging modality of choice in children[7]. However, SBFT requires high radiation dose with associated risks and, when possible, should be replaced by alternative techniques, such as low-dose CT or MRI[8-10], whose high accuracy is stated in the European Crohn's and Colitis Organization (ECCO) guidelines[10]. Particularly, ECCO guidelines, in the pediatric section[11,12], report dynamic contrast-enhanced MRI as the best imaging method to study CD's lesions. Also the Appropriateness Criteria of the American College of Radiology[13] confirm the high sensitivity and specificity of MRI (enterography or enteroclysis) in pediatric patients, similar to that of CT enterography but without the use of ionizing radiation.

However, many questions remain unsolved. First of all, it is important to determine whether these non-invasive imaging techniques can replace endoscopy in the evaluation of the mucosal healing. In a recent study, MRE has shown an accuracy of 90% and 84% in determining ulcer healing and endoscopic remission, respectively[14], but these data need to be confirmed.

In the last years, the eradication of bowel inflammation at the level of all wall layers has been suggested as a goal of treatment more appropriate than the mucosal healing alone that seems to be too superficial.

Compared to endoscopy, cross sectional imaging, especially MRI, can provide information on the entire bowel wall. However, transmural healing has not yet been studied as the primary therapeutic endpoint in CD patients, unlike the mucosal healing that is becoming more and more a therapeutic goal[15].

Preliminary studies have reported encouraging results on the diagnostic accuracy of DWI sequence in patients with IBD so that it can be considered, in the future, as an alternative to contrast-enhanced sequences[16,17].

Future studies should also consider the interobserver variability due to the different experience of radiologists in evaluating DWI images and standard MRI images.

Another concrete future possibility for the diagnosis and management of IBD is represented by the new hybrid imaging modalities, such as PET/CT and PET/MRI, which combine the morphological CT or MRI images with the functional PET information in a single diagnostic investigation. CT enterography combined

with the ^{18}F-FDG PET exam seems to be particularly promising[18].

Groshar *et al*[19] reported a good accuracy of PET/CT in the differential diagnosis between acute and chronic inflammation. Infact, they found an important relation between the maximum standardized uptake value [SUV(max)] and the mural CT patterns, such as submucosal edema or fat, expression of active and chronic inflammation, respectively. However, a high number of false positive results have been registered due to the physiologic ^{18}F-FDG uptake by the bowel wall[20,21]. Another important limitation is the high cumulative radiation dose required for the PET/CT exam, particularly because the IBD patients require numerous and repeated examinations[18].

Finally, no articles have been published on the use of PET/MRI in the diagnosis and follow up of IBD, even though this combined use of nuclear medicine and MRI, providing information on molecular and morphological events without the use of ionizing radiations, could change the future diagnostic approach. Infact, they seem to have high potential and can count on the advent of new MRI techniques, such as DWI and Spectroscopy, and new radiopharmaceuticals to label cells, such as radionuclides, fluorescent or bioluminescent markers (optical imaging) and MRI contrast agents (molecular MRI)[22]. A great hope is placed in this imaging investigation which could effectively help in the diagnosis and follow up of IBD providing information on involved inflammatory cells and cytokines.

REFERENCES

1 **Morse RW,** Cole LG. The anatomy of the normal small intestine as observed roentgenographically. *Radiology* 1927; **8:** 149-53 [DOI: 10.1148/8.2.149]

2 **Pesquera GS.** A method for the direct visualisation of lesions in the small intestine. *AJR* 1929; **22:** 254-7

3 **Moeschler O**, Mueller MK. Deep enteroscopy - indications, diagnostic yield and complications. *World J Gastroenterol* 2015; **21**: 1385-1393 [PMID: 25663758 DOI: 10.3748/wjg.v21.i5.1385]

4 **Stathaki MI**, Koukouraki SI, Karkavitsas NS, Koutroubakis IE. Role of scintigraphy in inflammatory bowel disease. *World J Gastroenterol* 2009; **15**: 2693-2700 [PMID: 19522018 DOI: 10.3748/wjg.15.2693]

5 **Louis E**, Ancion G, Colard A, Spote V, Belaiche J, Hustinx R. Noninvasive assessment of Crohn's disease intestinal lesions with (18)F-FDG PET/CT. *J Nucl Med* 2007; **48**: 1053-1059 [PMID: 17574978 DOI: 10.2967/jnumed.107.040436]

6 **Saboury B**, Salavati A, Brothers A, Basu S, Kwee TC, Lam MG, Hustinx R, Louis E, Torigian DA, Alavi A. FDG PET/CT in Crohn's disease: correlation of quantitative FDG PET/CT parameters with clinical and endoscopic surrogate markers of disease activity. *Eur J Nucl Med Mol Imaging* 2014; **41**: 605-614 [PMID: 24253895 DOI: 10.1007/s00259-013-2625-2]

7 **IBD Working Group of the European Society for Paediatric Gastroenterology, Hepatology and Nutrition**. Inflammatory bowel disease in children and adolescents: recommendations for diagnosis--the Porto criteria. *J Pediatr Gastroenterol Nutr* 2005; **41:** 1-7 [DOI: 10.1097/01.MPG.0000163736.30261.82]

8 **Desmond AN**, O'Regan K, Curran C, McWilliams S, Fitzgerald T, Maher MM, Shanahan F. Crohn's disease: factors associated with exposure to high levels of diagnostic radiation. *Gut* 2008; **57**: 1524-1529 [PMID: 18443021 DOI: 10.1136/gut.2008.151415]

9 **Gaca AM**, Jaffe TA, Delaney S, Yoshizumi T, Toncheva G, Nguyen G, Frush DP. Radiation doses from small-bowel follow-through and abdomen/pelvis MDCT in pediatric Crohn disease. *Pediatr Radiol* 2008; **38**: 285-291 [PMID: 18183380 DOI: 10.1007/s00247-007-0702-z]

10 **Panes J**, Bouhnik Y, Reinisch W, Stoker J, Taylor SA, Baumgart DC, Danese S, Halligan S, Marincek B, Matos C, Peyrin-Biroulet L, Rimola J, Rogler G, van Assche G, Ardizzone S, Ba-Ssalamah A, Bali MA, Bellini D, Biancone L, Castiglione F, Ehehalt R, Grassi R, Kucharzik T, Maccioni F, Maconi G, Magro F, Martín-Comín J, Morana G, Pendsé D, Sebastian S, Signore A, Tolan D, Tielbeek JA, Weishaupt D, Wiarda B, Laghi A. Imaging techniques for assessment of inflammatory bowel disease: joint ECCO and ESGAR evidence-based consensus guidelines. *J Crohns Colitis* 2013; **7**: 556-585 [PMID: 23583097 DOI: 10.1016/j.crohns.2013.02.020]

11 **Van Assche G**, Dignass A, Panes J, Beaugerie L, Karagiannis J, Allez M, Ochsenkühn T, Orchard T, Rogler G, Louis E, Kupcinskas L, Mantzaris G, Travis S, Stange E. The second European evidence-based Consensus on the diagnosis and management of Crohn's disease: Definitions and diagnosis. *J Crohns Colitis* 2010; **4**: 7-27 [PMID: 21122488 DOI: 10.1016/j.crohns.2009.12.003]

12 **Van Assche G**, Dignass A, Reinisch W, van der Woude CJ, Sturm A, De Vos M, Guslandi M, Oldenburg B, Dotan I, Marteau P, Ardizzone A, Baumgart DC, D'Haens G, Gionchetti P, Portela F, Vucelic B, Söderholm J, Escher J, Koletzko S, Kolho KL, Lukas M, Mottet C, Tilg H, Vermeire S, Carbonnel F, Cole A, Novacek G, Reinshagen M, Tsianos E, Herrlinger K, Oldenburg B, Bouhnik Y, Kiesslich R, Stange E, Travis S, Lindsay J. The second European evidence-based Consensus on the diagnosis and management of Crohn's disease: Special situations. *J Crohns Colitis* 2010; **4**: 63-101 [PMID: 21122490 DOI: 10.1016/j.crohns.2009.09.009]

13 **Huprich JE**, Rosen MP, Fidler JL, Gay SB, Grant TH, Greene FL, Lalani T, Miller FH, Rockey DC, Sudakoff GS, Gunderman R, Coley BD. ACR Appropriateness Criteria on Crohn's disease. *J Am Coll Radiol* 2010; **7**: 94-102 [PMID: 20142082 DOI: 10.1016/j.jacr.2009.10.009]

14 **Ordás I**, Rimola J, Rodríguez S, Paredes JM, Martínez-Pérez MJ, Blanc E, Arévalo JA, Aduna M, Andreu M, Radosevic A, Ramírez-Morros AM, Pinó S, Gallego M, Jauregui-Amezaga A, Ricart E, Panés J. Accuracy of magnetic resonance enterography in assessing response to therapy and mucosal healing in patients with Crohn's disease. *Gastroenterology* 2014; **146**: 374-82.e1 [PMID: 24177375 DOI: 10.1053/j.gastro.2013.10.055]

15 **Daperno M**, Castiglione F, de Ridder L, Dotan I, Färkkilä M, Florholmen J, Fraser G, Fries W, Hebuterne X, Lakatos PL, Panés J, Rimola J, Louis E. Results of the 2nd part Scientific Workshop of the ECCO. II: Measures and markers of prediction to achieve, detect, and monitor intestinal healing in inflammatory bowel disease. *J Crohns Colitis* 2011; **5**: 484-498 [PMID: 21939926 DOI: 10.1016/j.crohns.2011.07.003]

16 **Oussalah A**, Laurent V, Bruot O, Bressenot A, Bigard MA, Régent D, Peyrin-Biroulet L. Diffusion-weighted magnetic resonance without bowel preparation for detecting colonic inflammation in inflammatory bowel disease. *Gut* 2010; **59**: 1056-1065 [PMID: 20525970 DOI: 10.1136/gut.2009.197665]

17 **Neubauer H**, Pabst T, Dick A, Machann W, Evangelista L, Wirth C, Köstler H, Hahn D, Beer M. Small-bowel MRI in children and young adults with Crohn disease: retrospective head-to-head comparison of contrast-enhanced and diffusion-weighted MRI. *Pediatr Radiol* 2013; **43**: 103-114 [PMID: 23212595 DOI: 10.1007/s00247-012-2492-1]

18 **Shyn PB**, Mortele KJ, Britz-Cunningham SH, Friedman S, Odze RD, Burakoff R, Goldberg JE, Erturk M, Silverman SG. Low-dose 18F-FDG PET/CT enterography: improving on CT enterography assessment of patients with Crohn disease. *J Nucl Med* 2010; **51**: 1841-1848 [PMID: 21078803 DOI: 10.2967/jnumed.110.080796]

19 **Groshar D**, Bernstine H, Stern D, Sosna J, Eligalashvili M, Gurbuz EG, Niv Y, Fraser G. PET/CT enterography in Crohn disease: correlation of disease activity on CT enterography with 18F-FDG

uptake. *J Nucl Med* 2010; **51**: 1009-1014 [PMID: 20554741 DOI: 10.2967/jnumed.109.073130]

20 **Spier BJ**, Perlman SB, Jaskowiak CJ, Reichelderfer M. PET/CT in the evaluation of inflammatory bowel disease: studies in patients before and after treatment. *Mol Imaging Biol* 2010; **12**: 85-88 [PMID: 19430844 DOI: 10.1007/s11307-009-0232-1]

21 **Lemberg DA**, Issenman RM, Cawdron R, Green T, Mernagh J, Skehan SJ, Nahmias C, Jacobson K. Positron emission tomography in the investigation of pediatric inflammatory bowel disease. *Inflamm Bowel Dis* 2005; **11**: 733-738 [PMID: 16043988 DOI: 10.1097/01.MIB.0000172810.49619.cb]

22 **Cassidy PJ**, Radda GK. Molecular imaging perspectives. *J R Soc Interface* 2005; **2**: 133-144 [PMID: 16849174 DOI: 10.1098/rsif.2005.0040]

P- Reviewer: Djodjevic I, Suzuki H
S- Editor: Song XX **L- Editor**: A **E- Editor**: Jiao XK

World Journal of Radiology

Submit a Manuscript: http://www.wjgnet.com/esps/
Help Desk: http://www.wjgnet.com/esps/helpdesk.aspx
DOI: 10.4329/wjr.v7.i8.202

World J Radiol 2015 August 28; 7(8): 202-211
ISSN 1949-8470 (online)

MINIREVIEWS

Imaging of bone metastasis: An update

Gerard J O'Sullivan, Fiona L Carty, Carmel G Cronin

Gerard J O'Sullivan, Fiona L Carty, Carmel G Cronin, Department of Radiology, Mater Misericordiae University Hospital, Dublin 7, Ireland

Author contributions: O'Sullivan GJ, Carty FL and Cronin CG contributed equally to this work; O'Sullivan GJ wrote the paper.

Conflict-of-interest statement: None.

Correspondence to: Carmel G Cronin, MB, BCh, BAO, Consultant Radiologist, Department of Radiology, Mater Misericordiae University Hospital, Eccles Street, Dublin 7, Ireland. ccronin@mater.ie
Telephone: +353-1-8032274
Fax: +353-1-8032970

Received: July 17, 2014
Peer-review started: July 19, 2014
First decision: November 27, 2014
Revised: February 13, 2015
Accepted: June 18, 2015
Article in press: June 19, 2015
Published online: August 28, 2015

Abstract

Early detection of skeletal metastasis is critical for accurate staging and optimal treatment. This paper briefly reviews our current understanding of the biological mechanisms through which tumours metastasise to bone and describes the available imaging methods to diagnose bone metastasis and monitor response to treatment. Among the various imaging modalities currently available for imaging skeletal metastasis, hybrid techniques which fuse morphological and functional data are the most sensitive and specific, and positron emission tomography (PET)/computed tomography and PET/magnetic resonance imaging will almost certainly continue to evolve and become increasingly important in this regard.

Key words: Neoplasm metastasis; Radionuclide imaging; Magnetic resonance imaging; Computed tomography; Bone and bones

Core tip: Early detection of skeletal metastasis is critical for accurate staging and optimal treatment. This paper briefly reviews our current understanding of the biological mechanisms through which tumours metastasise to bone and describes the available imaging methods to diagnose bone metastasis and monitor response to treatment.

O'Sullivan GJ, Carty FL, Cronin CG. Imaging of bone metastasis: An update. *World J Radiol* 2015; 7(8): 202-211 Available from: URL: http://www.wjgnet.com/1949-8470/full/v7/i8/202.htm DOI: http://dx.doi.org/10.4329/wjr.v7.i8.202

INTRODUCTION

Metastasis of malignant neoplasms to bone is common with metastases being far more prevalent than primary bone malignancies[1,2]. Indeed, bone is the third most common organ affected by metastasis, surpassed only by the lungs and liver[2-4], and is the most common site of distant metastasis from primary breast carcinoma[5].

Over the past twenty years, advances in our understanding of tumour biology have led to the development of improved treatment strategies for many cancers. As a result, many patients are living longer with metastatic disease and the incidence of skeletal metastasis is continuing to rise. Based on post-mortem findings, approximately 70% of patients with breast or prostate

cancer have bone metastases[1,4]. Commensurate with the increased prevalence of bone metastasis, there is potential for significant comorbidities such as pain, limited mobility, hypercalcaemia, spinal cord or nerve root compression, myelosuppression and pathologic fracture[2,6]. Therefore, early detection of skeletal metastasis is critical for (1) accurate staging and optimal treatment; and (2) to allow the implementation of treatment strategies such as surgical fixation, radiotherapy, or bisphosphonate therapy to reduce the risk of complications and improve quality of life[7,8].

This paper briefly reviews our current understanding of the biological mechanisms through which tumours metastasise to bone and describes the available imaging methods to diagnose bone metastasis and monitor response to treatment.

PATHOPHYSIOLOGY OF BONE METASTASIS

Certain primary malignant neoplasms such as breast carcinoma and prostate adenocarcinoma have a propensity for metastasising to bone and are, therefore, termed osteotropic. Conversely, patients with cervical, endometrial, bladder and gastrointestinal tract tumours rarely develop skeletal metastases[9]. The selective deposition and proliferation of discrete circulating malignant cells within the skeleton relates to the "seed and soil" hypothesis of tumour biology originally conceptualised by Stephen Paget in the late 19th century. In accordance with this hypothesis, the bone environment represents a "fertile soil" in which some, but not all, cancer cell types (seeds) can flourish.

Metastasis to bone can occur *via* direct extension, arterial or venous spread with the latter representing the most common form. Once in the circulation, entry of the cancer cells into the venous circulation of the bone marrow is facilitated by the slow blood flow and the fact that hematopoietically active bone marrow is well vascularised[1]. Adhesion molecules produced by tumour cells bind to marrow stromal cells and bone matrix[8]. The normal remodelling process of bone provides chemotactic and growth factors which support these cancer cells once in place[1]. After skeletal colonisation, the malignant cells interrupt normal bone cell turnover by releasing local cytokines and growth factors. Certain tumours release factors which upregulate osteoclast activity such as parathyroid hormone-related protein, tumour necrosis factor α or β, and other cytokines such as interleukin-1 and interleukin-6 which results in net osteolysis. Other cancer cell types release factors such as epidermal growth factor, transforming growth factor α and β, and insulin-like growth factors which upregulate osteoblasts resulting in net osteosclerosis[8,10]. Thus, osseous metastases can be osteoblastic (bone forming) or osteolytic (bone destructive), however, a combination of both processes occurs in most cancers[4]. Osseus metastases from kidney, thyroid and lung malignancies are predominantly osteolytic, while osteoblastic lesions are usually seen in prostate cancer and breast cancer[7]. Furthermore, osteolytic metastases tend to be aggressive, whereas sclerotic metastases typically demonstrate slower progression. An important point to realise is that tumour cell proliferation within the bone marrow invariably predates bone destruction which is, consequently, a relatively delayed manifestation in bone metastasis which has important implications in terms of diagnosis[6].

DISTRIBUTION OF BONE METASTASIS

Considering benign osseous lesions and bone metastases oftentimes have similar imaging features, the location of a lesion in the skeleton can sometimes be used to help distinguish between the two in equivocal cases. The vertebrae, pelvis, ribs and the ends of long bones are preferred destinations of metastases because of their high red marrow content[1,9,11]. Within the spine, most metastases are located in the lumbar spine, less frequently in the thoracic spine, and rarely in the cervical spine (52%, 36% and 12% respectively)[12]. Less frequent metastatic sites include the mandible, patella, and dital extremities. In the majority of instances, metastases in the appendicular skeleton are secondary to lung cancer and are typically located in the scaphoid, lunate or phalanges[7] (Figure 1).

PLAIN FILM

Plain radiographs are recommended to assess abnormal radionuclide uptake or the risk of pathological fracture and as initial imaging studies in patients with bone pain[5]. However, radiography is considered insensitive to screen for asymptomatic metastases[9]. Limited contrast in trabecular bone vis a vis cortical bone renders radiographic detection of lesions in the former more difficult and studies have shown that more than 50% to 70% of bone must be destroyed to be reliably detected by plain radiographs[2,7]. Osteolytic lesions typically demonstrate thinning of trabeculae and ill-defined margins with the latter representing abnormal trabeculae between the centre of the lesion and the radiologically normal bone. Conversely, sclerotic metastases classically appear as nodular, rounded and fairly well circumscribed lesions secondary to thickened coarse trabeculae[8].

Skeletal metastases may respond to treatment with reactive new bone formation, or sclerosis. Sclerosis tends to be initiated at the margins of the lesion and progress over time towards the centre. Sclerotic change in an osteolytic metastasis usually indicates a healing response to therapy, whereas worsening or developing osteolysis within sclerotic or mixed lesions, or progressive enlargement of an existing lesion, are indicators of disease progression[7]. Disadvantages of plain film for monitoring

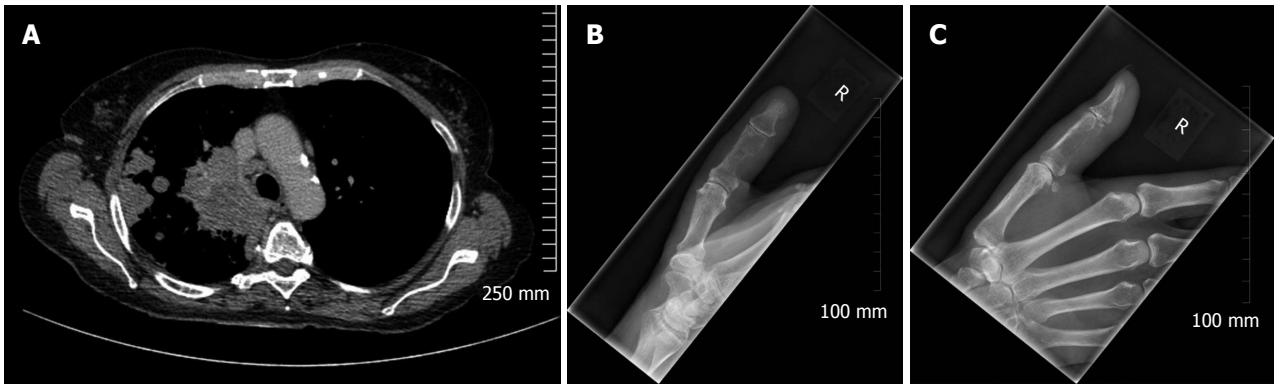

Figure 1 Bone metastasis in the appendicular skeleton is most commonly due to primary lung malignancy. A: Axial computed tomography image of the upper thorax (soft tissue window) demonstrating a large right upper lobe mass with ipsilateral pulmonary and lymph node metastasis; B and C: PA and lateral views of the right thumb demonstrating a lytic metastatic deposit in the middle phalanx.

Table 1 Sensitivity and specificity of imaging modalities in bone metastasis

Imaging modality	Sensitivity (%)[12]	Specificity (%)[12]
18F NaF-PET/CT	100	97
MRI	95	90
SPECT	87	91
18F FDG-PET	98	56
CT	74	56
Bone Scintigraphy	78	48

PET: Positron emission tomography; CT: Computed tomography; MRI: Magnetic resonance imaging; SPECT: Single photon emission tomography; 18F FDG: Fluorine 18 labelled fluorodeoxyglucose; 18F NaF: Fluorine 18 labelled sodium fluoride.

treatment response are that (1) typically 3-6 mo are required before any changes manifest radiographically; and (2) plain films only reveal structural bone alterations, and do not provide information on the malignant cells within the metastatic soft tissue deposit. Furthermore, differentiating new sclerotic metastases secondary to disease progression from sclerotic lesions caused by healing and re-ossification is often challenging[3,6].

COMPUTED TOMOGRAPHY

Computed tomography (CT) provides excellent resolution of cortical and trabecular bone and is the imaging modality of choice for evaluating the ribs which have a high cortex to marrow ratio. The ability to apply dedicated bone algorithms to acquired images, adjust the window width and level, and view the skeleton in multiple planes using multiplanar reformatted images all serve to maximise the conspicuity of bone lesions and results in a higher sensitivity of CT compared to plain radiography in detecting both osteolytic and osteosclerotic metastases. The sensitivity and specificity of CT for detection of bone metastasis is 74% and 56%, respectively (Table 1). A major advantage of CT is that investigation for skeletal metastasis or evaluating treatment response can be performed at the time of staging or restaging other organs which reduces the burden of imaging for the patient. Despite the limited soft tissue resolution of CT vis a vis magnetic resonance imaging (MRI), in many instances, CT can demonstrate bone marrow metastases before bone destruction occurs which results in earlier diagnosis and can improve prognosis and prevent complications[6]. A further advantage of CT is that it can used to guide percutaneous biopsy when a tissue diagnosis is required[7].

Clinical trials have demonstrated a role for CT in evaluating for sclerotic change within a metastatic deposit which can occur in response to treatment of skeletal metastases with chemo/radiotherapy. Specifically, reactive sclerosis may be quantified by calculating the change in Hounsfield units within metastatic deposits following bisphosphonate therapy, thereby providing a valid objective measure of treatment response[3].

MRI

Due to its excellent soft tissue resolution, MRI is the imaging modality of choice for assessing metastatic spread in the marrow cavity, extension of tumour from the marrow cavity and involvement of surrounding structures[5]. Furthermore, MRI is highly sensitive for detecting skeletal metastasis as it has the capability to demonstrate an intramedullary metastatic deposit in advance of cortical destruction occurs and before a pathologic osteoblastic process manifests as focal accumulation of radiotracer on a bone scan (Figure 2)[6,8]. The sensitivity and specificity of MRI for detection of bone metastasis is 95% and 90%, respectively (Table 1). In addition, MRI is the technique of choice in suspected cases of cord compression from pathologic vertebral body fracture where a compromised oedematous spinal cord will demonstrate abnormal focal high T2 and turbo-short tau inversion recovery (STIR) signal. Given that MRI does not involve ionising radiation, it is especially suited for the investigation of suspected bony metastasis in pregnant women.

Normal bone marrow contains a high percentage

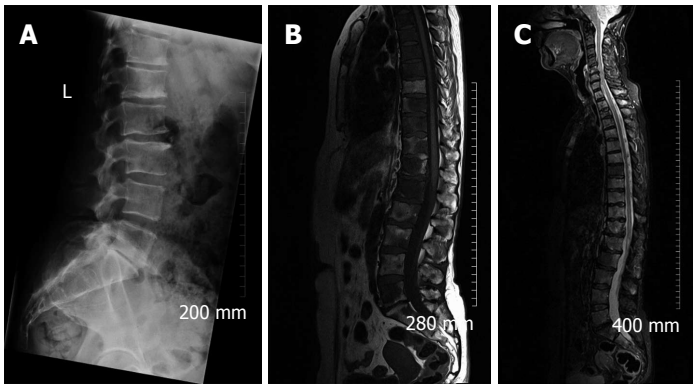

Figure 2 Magnetic resonance imaging is superior to plain radiography for detection of bone metastasis. A: Lateral lumbar spine radiograph demonstrates subtle sclerotic metastatic deposits at the inferior endplate of T12 and L1 from a primary breast malignancy; Sagittal T1 (B) and short tau inversion recovery (STIR) (C) images of the spine acquired one day later demonstrate diffuse bone metastasis (abnormal low T1 and high STIR signal in the bone marrow) which is not evident on the radiograph.

of fat and demonstrates high signal intensity on T1-weighted sequences. Osseous metastases usually manifest as discrete foci of low T1 signal, corresponding to the replacement of normal fatty marrow by malignant cells. On a T2-weighted sequence, bone metastases usually demonstrate T2 hyperintensity due to their elevated water content and gadolinium enhancement due to increased vascularity[4,7].

The development of whole-body MRI in recent years, which uses fast pulse sequences over multiple anatomic stations to achieve a survey of the entire body, has resulted in the ability to use unenhanced T1-weighted spin echo and STIR sequences to screen the whole body for marrow abnormalities with a sensitivity and specificity superior to skeletal scintigraphy[5-7]. One limitation of MRI is that cortical bone, with its very short T2 relaxation time, is very poorly interrogated. Therefore, bones with a low marrow volume such as the ribs are better evaluated with CT as described above[6].

An advantage of MRI is that it can sometimes be used to distinguish osteoporotic from malignant vertebral compression fractures. Oedema from osteoporotic compression fractures should subside in within 3 mo. If marrow oedema persists on a follow-up MRI study performed at least 12 wk after the initial scan, a pathologic fracture is likely[5], however, this correlation can be inconsistent and determining if marrow signal changes are due to fracture or tumour remains a diagnostic challenge using MRI alone[4].

MRI can be used to assess treatment response by evaluating the size and number of osseous metastases over time. It is important to note, however, that alteration in signal intensity alone on a T1-weighted sequence does not constitute a response to therapy. Recent studies suggest that quantitative diffusion weighted imaging (DWI) can be used to evaluate treatment response before a change in the tumour burden can be seen using non quantitative assessment. More specifically, early reduction in tumour cell volume following cell death with a corresponding increase in the extracellular space is manifested on DWI as an increase in the apparent diffusion coefficient (ADC) value of the metastatic deposit[6]. However, further studies are needed to define the precise imaging criteria, for example T1 and DWI signal characteristics and/or percentage signal change pre and post contrast, which should be used to evaluate the treatment response[3].

NUCLEAR MEDICINE

Morphological imaging techniques such as plain film, CT and MRI described above interrogate the structure of a lesion within bone. Conversely, nuclear medicine techniques quantitatively assess the function of bone or tumour cells[6]. Prior to describing the role of the nuclear medicine imaging modalities most commonly used for imaging skeletal metastases, it is pertinent to briefly review the various radioisotopes that are employed in these studies. For more comprehensive coverage of this topic the reader is referred to the recent review by Cuccurullo *et al*[2].

Osteotropic radioisotopes are bone seeking agents that accumulate at the site of active bone production regardless of whether the aetiology is benign or malignant. The predominant osteotropic agents used in skeletal scintigraphy are metastable technetium 99 labelled diphosphonates, among which methylene diphosphonate (99mTc-MDP) is used most commonly based on its effectiveness, low cost, widespread availability and favourable dosimetry. 18Flabelled sodium fluoride (NaF) is an osteotropic compound used in positron emission tomography (PET) which has a higher first pass extraction rate than 99mTc-MDP. Indeed, studies indicate that the regional extraction of 18F NaF from plasma to bone is on average approximately three times higher in metastatic lesions than in adjacent normal bone tissue. Consequently, 18F NaF has very high selectivity for bone metastases, however its relatively low specificity when not used in conjunction with morphological imaging techniques (see hybrid

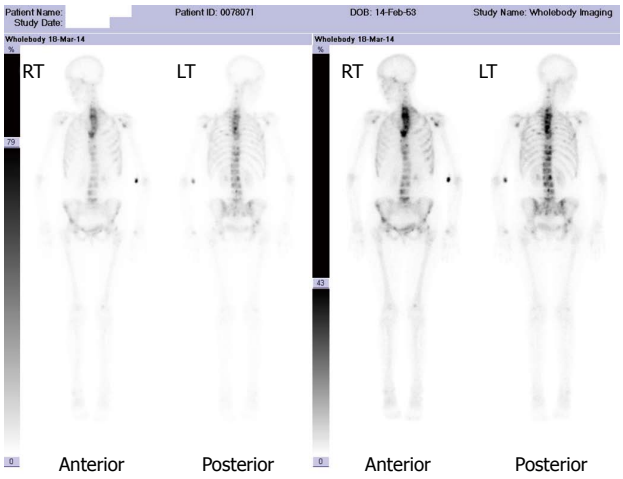

Figure 3 Diffuse bone metastasis on bone scintigraphy. Abnormal accumulation of radiotracer throughout the spine, most pronounced in the upper thoracic spine with additional pelvic and bilateral rib metastases in a patient with primary breast malignancy. Focal accumulation of radiotracer in the left antecubital fossa represents artefact at the radiotracer injection site.

imaging below) and the requirement of a cyclotron for production are limiting factors in its use[2].

In contrast to osteotropic agents, which have a high affinity for calcium, oncotropic radioisotopes demonstrate uptake into malignant cells and are classified as either specific or non-specific. Specific oncotropic agents are available to investigate for bone metastases from neuroendocrine tumours. For example, metaiodobenzylguanidine is a noradrenaline analogue, taken up specifically by the sympathetic nervous system and related tumours. When labelled with Iodine 123 or Iodine 131 it may detect bone metastases from pheochromocytomas and paragangliomas. In addition, somatostatin receptor scintigraphy with Indium 111 pentetreotide (octreoscan) and PET-CT using Gallium 68 labelled somatostatin analogues can be used to diagnose both organ confined and metastatic neuroendocrine malignancies. Further information regarding available specific oncotropic tracers can be found on the Molecular Imaging and Contrast Agent Database http://www.ncbi.nlm.nih.gov details. The most commonly used non-specific oncotropic radioisotope is the glucose analogue 18F labelledfluorodeoxyglucose (18F FDG). Uptake of 18F FDG occurs in cells with increased glucose metabolism such as neurons and mitotic neoplastic cells. Therefore, similar to osteotropic compounds, and as their name suggests, non-specific oncotropic radioisotopes are sensitive but not specific for skeletal metastasis.

SKELETAL SCINTIGRAPHY

Bone scintigraphy continues to be the most widely used radionuclide technique for investigation of skeletal metastasis primarily due to its widespread availability[2]. Radiotracer uptake depends on local blood flow, osteoblastic activity and extraction efficiency. Once accumulated in bone diphosphonates are absorbed by hydroxyapatite crystals on mineralizing bone surfaces[13].

A major advantage of radionuclide bone scanning is that imaging of the whole skeleton can be performed (Figure 3). This is important given that metastatic lesions can occur in regions of the appendicular skeleton that are not routinely included in a skeletal survey[9]. A further advantage relates the high sensitivity of scintigraphy which enables earlier detection of osseous metastases. The sensitivity and specificity of bone scintigraphy for detection of bone metastasis is 78% and 48%, respectively (Table 1). In particular, studies indicate that only a 5%-10% alteration in the ratio of lesion to normal bone is necessary to manifest abnormal tracer accumulation on a bone scan. As a result, osteosclerotic bone metastases can be detected on bone scintigraphy up to 18 mo earlier than on plain radiographs[7].

Skeletal scintigraphy has some notable limitations. For example, bone scintigraphy is non-specific and multiple benign osseous lesions, such as eosinophilic granuloma fibrous dysplasia and enchondroma, can lead to a false positive diagnosis of bone metastasis[14]. Interpreting focal accumulation of radiotracer in the spine can be particularly problematic as degenerative disease may be indistinguishable from bone metastases. Consequently, other imaging modalities such as plain radiography, CT or MRI are often required for correlation to exclude benign causes[8]. Secondly, the spatial resolution of scintigraphy is poor measuring approximately 1 cm and can result in difficulty determining the precise location of a lesion within a bone which can be of diagnostic significance[2]. Thirdly, bone scintigraphy assesses osteoblastic processes rather than tumour proliferation and, consequently, false negative results can occur[8]. Furthermore, primarily osteolytic lesions with limited reactive osteoblastic reaction, such as renal cell carcinoma metastases, typically demonstrate low or absent tracer accumulation leading to a false negative result (Figure 4)[6]. Finally, when bone metastases are extensive and diffuse, a bone scan on first inspection may appear normal due to the confluent nature of the lesions (referred to as a super scan because of the apparent good quality of the scan) and can be misinterpreted as a negative study[9,13]. It is therefore import to carefully assess for uptake in the kidneys on skeletal scintigraphy indicative of renal excretion of radiotracer which is characteristically absent on a super scan.

Certain clues and techniques can help to determine if focal uptake of radiotracer is secondary to a benign osseous lesion or metastasis. For example, vertebral body fractures have a characteristic appearance on bone scintigraphy, showing a horizontal linear pattern of increased tracer accumulation. Multiple linear abnormalities of varying intensity favour a benign aetiology with presumed osteoporotic fracture occurring at different time points. In addition, a short interval follow-up scan that shows reducing activity at a vertebral fracture site

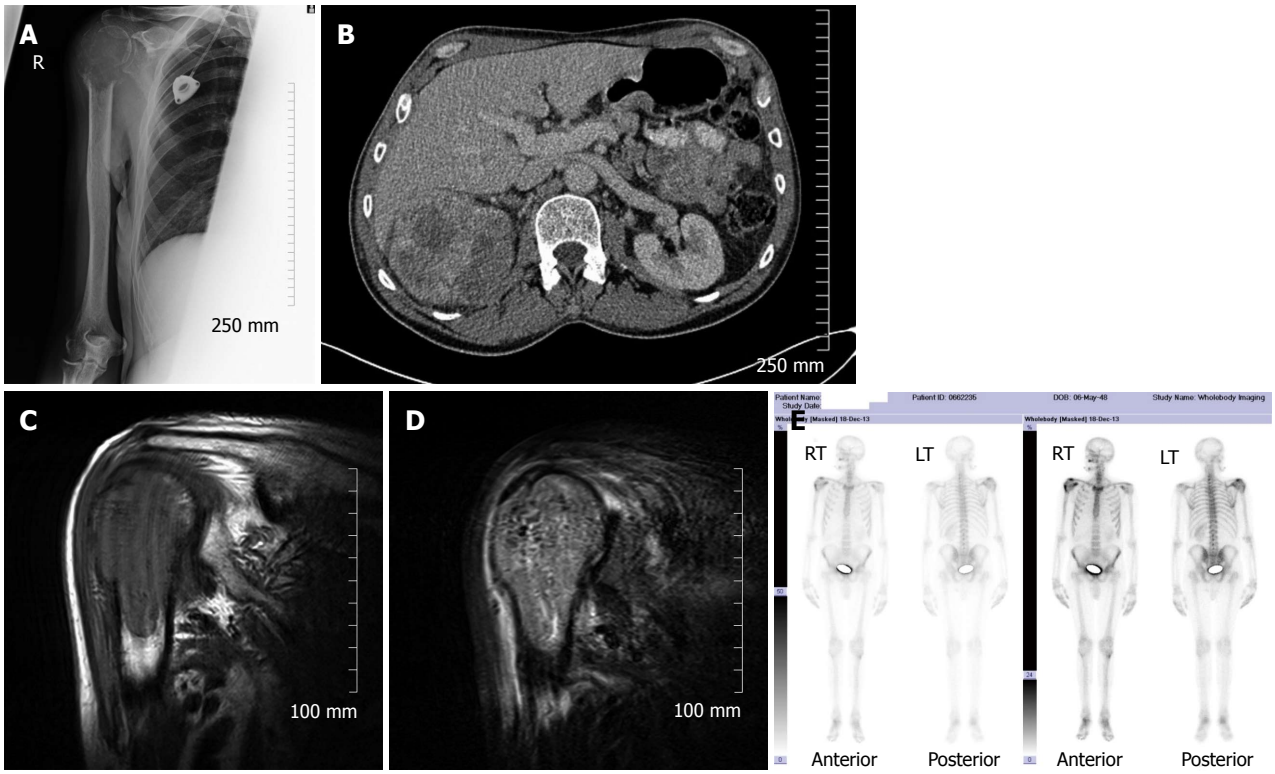

Figure 4 Lytic bone metastases are poorly demonstrated on bone scintigraphy. Plain radiograph (A) demonstrating a lytic metastatic deposit in the right proximal humerus in a patient with a large right renal cell carcinoma (B); Corresponding abnormal low T1 and high short tau inversion recovery signal on magnetic resonance imaging (C and D); Only the small osteoblastic component of the metastatic deposit demonstrates abnormal accumulation of radiotracer on bone scintigraphy (E).

suggests a benign aetiology and a healing fracture. Secondly, lesions that extend from the vertebral body into the posterior vertebral elements or involve the pedicle are more likely to represent metastases[13]. Finally, linear uptake of radiotracer in contiguous ribs is highly suggestive of trauma and not metastasis.

Bone metastases responding to treatment will demonstrate reduced or absent radiotracer uptake when compared with the pretreatment scan[6]. It is important to recognise, however, that early in the course of treatment a flare response can occur, which is characterized by a transient elevation in radiotracer accumulation secondary to the stimulation of osteoblasts during the repair process which can be misinterpreted as treatment failure, as it can have an imaging appearance indistinguishable from disease progression[7]. The flare response is most commonly associated with hormone based therapies and may last for up to 6 mo after therapy[13]. Progression of disease is suggested when new deposits develop or there is an interval increase in the is activityor size of existing deposits[3].

SINGLE PHOTON EMISSION CT

Single photon emission CT (SPECT) imaging of the skeleton uses 99mTc-MDP, the same radionuclide used in conventional skeletal scintigraphy, however images are acquired in a cross-sectional rather than a planar fashion. Whereas planar imaging is limited by superimposition of structures, SPECT can show axial slices through the body, providing better localisation of abnormal radionuclide uptake[5,7]. The sensitivity and specificity of SPECT for detection of bone metastasis is 87% and 91%, respectively (Table 1). A limitation of SPECT when compared with other available nuclear medicine technique is an inability to generate absolute quantification values[6].

PET

PET is a nuclear medicine technique that produces high-resolution tomographic images through the detection of high-energy photon pairs emitted during positron decay of a radioisotope. PET is superior to conventional bone scanning in terms of spatial resolution. For skeletal metastases, 18F NaF or 18F FDG are the radiopharmaceuticals most frequently employed[7].

The uptake mechanism of 18F NaF is similar to that of 99mTc-MDP. Specifically, following diffusion through the capillary wall into the extracellular fluid, fluoride ions undergo gradual exchange with the hydroxyl groups of hydroxy-apatite crystal within bone to form fluoro-apatite and subsequently deposited primarily on the surface of bone where re-modelling is maximal. Therefore, 18F NaF-PET demonstrates radiotracer accumulation at foci of osteoblastic activity[6,7]. The available literature indicates that 18F NaF-PET is substantially more sensitive and specific than skeletal

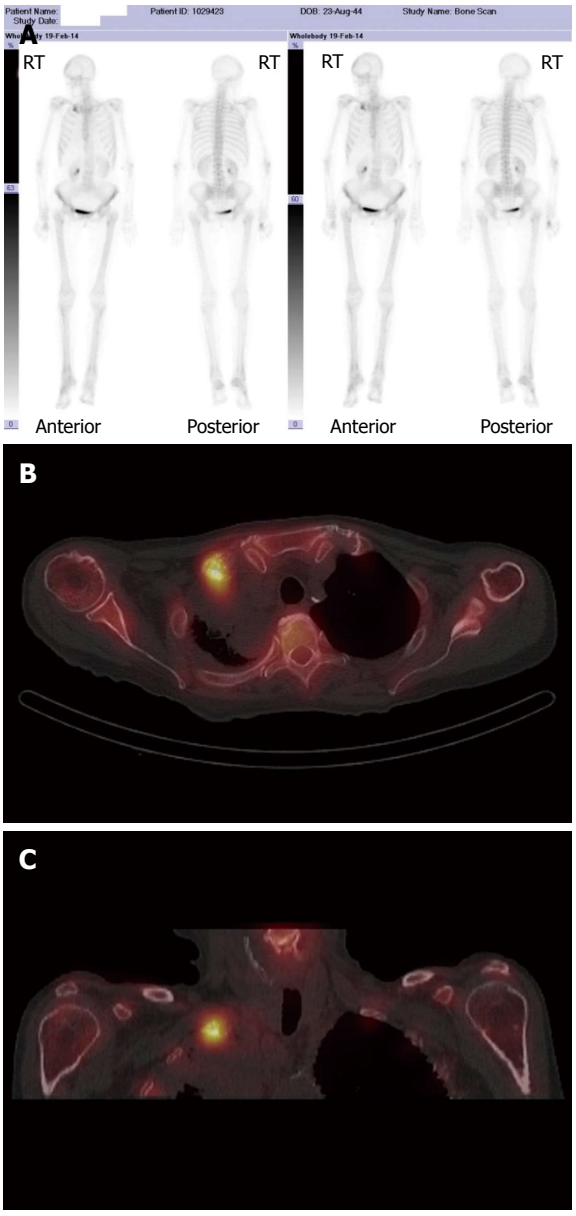

Figure 5 Single photon emission computed tomography has higher sensitivity and specificity for detection of bone metastasis when compared with bone scinitigraphy. A: Abnormal accumulation of radiotracer in the right clavicle on bone scintigraphy in a patient with primary lung malignancy; Axial (B) and coronal (C) single photon emission CT/CT images demonstrate the superior spatial and contrast resolution of this hybrid technique which enables improved detection and characterisation on bone metastases.

scintigraphy and SPECT for detection of metastases, particularly for osteolytic lesions[4,15]. In addition, comparative studies have demonstrated that 18F NaF-PET demonstrates higher sensitivity for detection of bone lesions when compared with 18F FDG-PET[8].

18F FDG-PET is a functional rather than anatomic imaging method that detects cellular metabolism of a glucose analogue. Many radiopharmaceuticals are available that can be imaged with PET, but 18F FDG is commonly used in oncology because of the high glucose uptake by many tumours[5]. Accumulation of 18F FDG is predominantly related to the amount of viable tumour cells. However, the sensitivity of 18F FDG-PET may vary among different histologies[4]. For example, it has been established that certain well-differentiated and indolent tumours, such as neuroendocrine and bronchial tumours, go undetected by 18F FDG because of the poor 18F FDG accumulation. Furthermore, in patients with primarily osteosclerotic metastases from prostate cancer, 18F FDG-PET has reduced sensitivity for the detection of skeletal metastases compared with 99mTc-MDP scintigraphy[6]. This is due to the reduced metabolic activity in sclerotic bone metastases. The sensitivity and specificity of 18F FDG-PET for detection of bone metastasis is 98% and 56%, respectively (Table 1).

A major advantage of 18F FDG-PET is the ability to compare the maximum standardised uptake value of a metastatic skeletal deposit between studies which provides an objective measure of the response to treatment. However, similar to skeletal scintigraphy, a potential limitation of 18F FDG-PET in assessing the treatmentresponse of metastatic bone disease is the flare phenomenon (described above) which may be seen after hormone therapy, which can be challenging to distinguish from bone marrow replacement by malignant cells, and result in false positive findings[3,6].

HYBRID IMAGING TECHNIQUES

It is clear from the preceding sections that the various imaging modalities traditionally used to investigate skeletal metastasis have idiosyncratic strengths and weaknesses. For example, an alteration in the structure of bone in response to treatment may be well demonstrated on CT, whereas tumour cell response is usually best evaluated using PET[6]. It is intuitive, therefore, that combining imaging modalities can increase sensitivity and specificity to improve diagnostic accuracy. The sensitivity and specificity of 18F NaF-PET/CT for detection of bone metastasis is 100% and 97%, respectively (Table 1). Indeed, technological advances have enabled the development of hybrid imaging techniques including SPECT/CT, PET/CT (Figures 5 and 6) and, more recently, PET/MRI. These techniques are (semi-) quantitative providing a standardized uptake value and allow the fusion of anatomic data from cross sectional imaging with functional information from nuclear medicine studies. As a result, the radiologist can determine if focal radiotracer uptake on a nuclear medicine study corresponds to a discrete skeletal lesion. Similarly, diagnostic confidence increases when an osseous lesion suspicious for metastasis on cross sectional imaging avidly accumulates radiotracer. A recent meta-analysis by Liu *et al*[16] found that 18F FDG-PET was the best modality to detect bone metastasis in patients with lung cancer, both on a per-patient and per-lesion basis while MRI had the highest specificity on a per-lesion basis. Furthermore, PET/CT was shown to be better than PET alone.

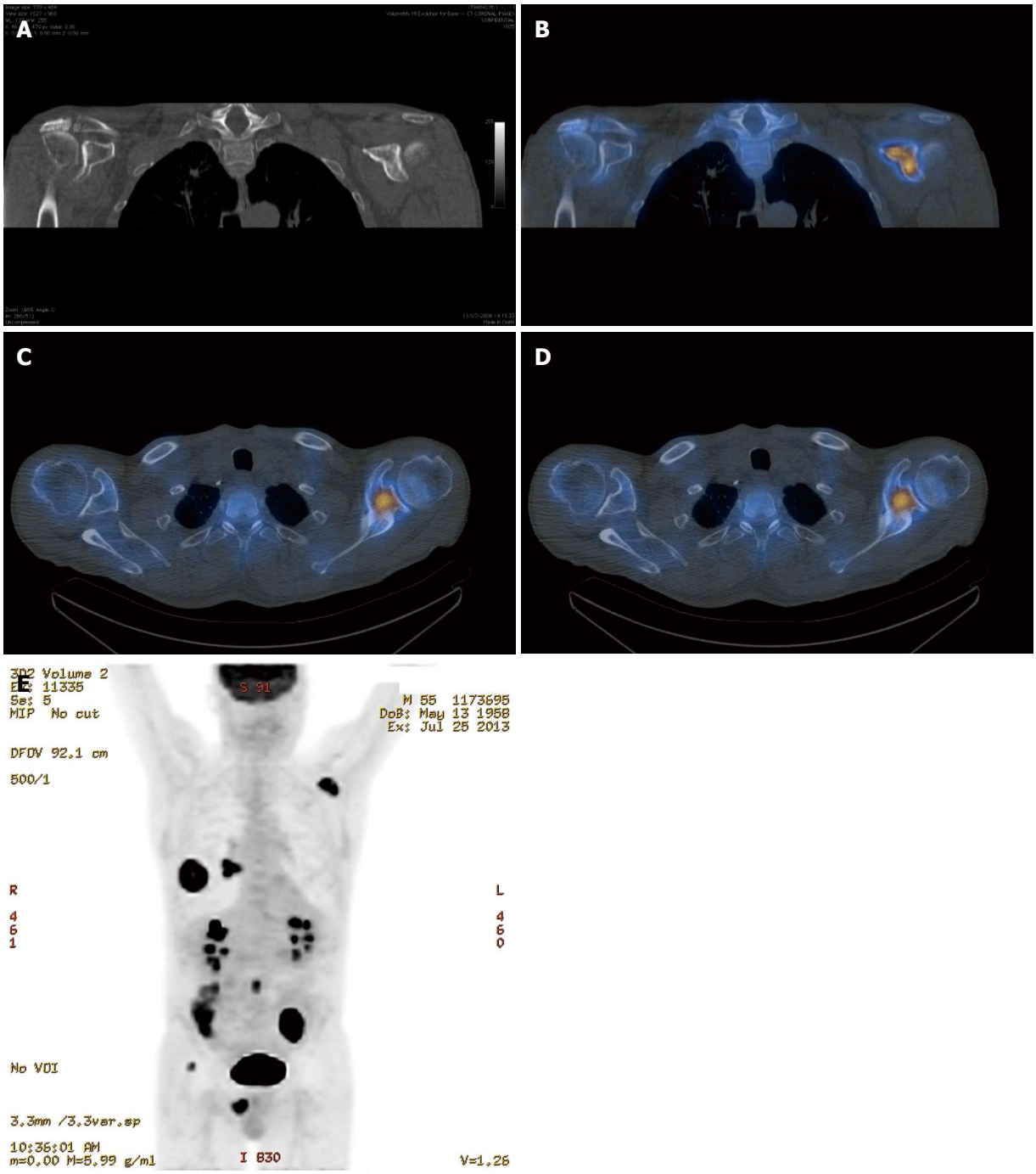

Figure 6 Single photon emission emission computed tomography-computed tomography is more sensitive for detection of bone metastasis than computed tomography alone. A: Coronal CT image of the left scapula (bone window) in a patient with primary lung malignancy does not demonstrate an aggressive bone lesion; Coronal and axial single photon emission CT/CT (B, C) and axial 18F fluorodeoxyglucose-positron emission tomography (FDG-PET)/CT (D) demonstrate abnormal radiotracer accumulation in the left clavicle consistent with bone metastasis; E: Coronal PET maximum intensity projection image demonstrating 18F FDG avid primary lung malignancy and right hilar lymph node metastasis in addition to the metastatic deposit in the left scapula.

The highest potential for early diagnosis of skeletal metastasis should, therefore, involve a combination of MRI and PET. To our knowledge, there is currently no published article comparing the accuracy of PET/CT and PET/MRI in diagnosing skeletal metastases and work in this area is warranted. One disadvantage of the hybrid imaging techniques involving CT is the radiation dose incurred by the patient, with a typical effective dose of approximately 22 mSv[5]. A low dose CT protocol can be used without significantly affecting the improved spatial localisation afforded by PET/CT *vs* PET alone, however, much of the precise anatomic detail is lost. Recent improvements in iterative reconstruction techniques are enabling low dose image acquisition while maintaining excellent contrast resolution and continued progress in this regard is likely.

EXPERIMENTAL IMAGING OF BONE METASTASIS

In this overview of imaging skeletal metastasis, it seems appropriate to briefly highlight experimental imaging strategies currently being explored that may influence the future of oncologic imaging.

Optical imaging techniques which involve transgenic expression of bioluminescent or fluorescent proteins in cancer cell lines are yielding novel information on how tumour cells invade, spread, proliferate and respond to treatment in small animal models of bone metastasis[17,18]. While such advances are critical to advancing our understanding of tumour biology, it will likely take many years before the results of this research manifest clinically.

Imaging research focused on tumour stimulated angiogenesis may well lead to improvements in imaging skeletal metastasis in the near future. Vascularity of osseous metastases can be visualised by cross sectional imaging and quantitative data obtained. Specifically, dynamic contrast-enhanced (DCE) MRI or CT can be employed to quantify variables in tissue vascularity, such as blood volume and perfusion. DCE imaging can be achieved by sequentially imaging the distribution of a systemically administered contrast agent producing imaging biomarkers that which can then be used to evaluate the response of a tumour to therapies designed to inhibit angiogenesis. Using this approach, potential treatment responses can be detected at an early stage using MRI and CT, before a change in the tumour volume can be reliably detected[6]. Therefore, DCE will likely continue to develop as a sensitive method to evaluate early tumour response.

CONCLUSION

The availability of improved chemotherapy regimens for many cancers together with a more aggressive approach by surgical oncologists means that many patients are now living longer with metastatic disease. Prolonged survival of patients with cancer results in a greater likelihood of developing distant metastasis which has, in turn, led to a higher prevalence of skeletal metastasis[19]. In line with these changes, considerable advances in imaging technology have enabled more reliable evaluation of bone metastases and treatment response. Among the various imaging modalities currently available for imaging skeletal metastasis, hybrid techniques which fuse morphological and functional data are the most sensitive and specific, and PET/CT and PET/MRI will almost certainly continue to evolve and become increasingly important in this regard. At present, however, no single imaging strategy is consistently superior for the assessment of metastatic bone disease across all tumour types and clinical scenarios[9]. The future of imaging bone metastasis will likely involve the development of an array of new radiotracers which will be tumour specific and greatly increase diagnostic accuracy.

REFERENCES

1 **Bussard KM**, Gay CV, Mastro AM. The bone microenvironment in metastasis; what is special about bone? *Cancer Metastasis Rev* 2008; **27**: 41-55 [PMID: 18071636 DOI: 10.1007/s10555-007-9109-4]

2 **Cuccurullo V**, Cascini GL, Tamburrini O, Rotondo A, Mansi L. Bone metastases radiopharmaceuticals: an overview. *Curr Radiopharm* 2013; **6**: 41-47 [PMID: 23470032 DOI: 10.2174/1874471011306010007]

3 **Vassiliou V**, Andreopoulos D, Frangos S, Tselis N, Giannopoulou E, Lutz S. Bone metastases: assessment of therapeutic response through radiological and nuclear medicine imaging modalities. *Clin Oncol* (R Coll Radiol) 2011; **23**: 632-645 [PMID: 21530193 DOI: 10.1016/j.clon.2011.03.010]

4 **Yu HH**, Tsai YY, Hoffe SE. Overview of diagnosis and management of metastatic disease to bone. *Cancer Control* 2012; **19**: 84-91 [PMID: 22487970]

5 **Costelloe CM**, Rohren EM, Madewell JE, Hamaoka T, Theriault RL, Yu TK, Lewis VO, Ma J, Stafford RJ, Tari AM, Hortobagyi GN, Ueno NT. Imaging bone metastases in breast cancer: techniques and recommendations for diagnosis. *Lancet Oncol* 2009; **10**: 606-614 [PMID: 19482249 DOI: 10.1016/S1470-2045(09)70088-9]

6 **Bäuerle T**, Semmler W. Imaging response to systemic therapy for bone metastases. *Eur Radiol* 2009; **19**: 2495-2507 [PMID: 19468736 DOI: 10.1007/s00330-009-1443-1]

7 **Choi J**, Raghavan M. Diagnostic imaging and image-guided therapy of skeletal metastases. *Cancer Control* 2012; **19**: 102-112 [PMID: 22487972]

8 **Rajarubendra N**, Bolton D, Lawrentschuk N. Diagnosis of bone metastases in urological malignancies--an update. *Urology* 2010; **76**: 782-790 [PMID: 20346492 DOI: 10.1016/j.urology.2009.12.050]

9 **Roberts CC**, Daffner RH, Weissman BN, Bancroft L, Bennett DL, Blebea JS, Bruno MA, Fries IB, Germano IM, Holly L, Jacobson JA, Luchs JS, Morrison WB, Olson JJ, Payne WK, Resnik CS, Schweitzer ME, Seeger LL, Taljanovic M, Wise JN, Lutz ST. ACR appropriateness criteria on metastatic bone disease. *J Am Coll Radiol* 2010; **7**: 400-409 [PMID: 20522392 DOI: 10.1016/j.jacr.2010.02.015]

10 **Longo V**, Brunetti O, D'Oronzo S, Ostuni C, Gatti P, Silvestris F. Bone metastases in hepatocellular carcinoma: an emerging issue. *Cancer Metastasis Rev* 2014; **33**: 333-342 [PMID: 24357055 DOI: 10.1007/s10555-013-9454-4]

11 **Saha S**, Burke C, Desai A, Vijayanathan S, Gnanasegaran G. SPECT-CT: applications in musculoskeletal radiology. *Br J Radiol* 2013; **86**: 20120519 [PMID: 24096590 DOI: 10.1259/bjr.20120519]

12 **Talbot JN**, Paycha F, Balogova S. Diagnosis of bone metastasis: recent comparative studies of imaging modalities. *Q J Nucl Med Mol Imaging* 2011; **55**: 374-410 [PMID: 21738113]

13 **Gnanasegaran G**, Cook G, Adamson K, Fogelman I. Patterns, variants, artifacts, and pitfalls in conventional radionuclide bone imaging and SPECT/CT. *Semin Nucl Med* 2009; **39**: 380-395 [PMID: 19801218 DOI: 10.1053/j.semnuclmed.2009.07.003]

14 **Zhang Y**, Zhao C, Liu H, Hou H, Zhang H. Multiple metastasis-like bone lesions in scintigraphic imaging. *J Biomed Biotechnol* 2012; **2012**: 957364 [PMID: 22505821 DOI: 10.1155/2012/957364]

15 **Yang HL**, Liu T, Wang XM, Xu Y, Deng SM. Diagnosis of bone metastases: a meta-analysis comparing ^{18}FDG PET, CT, MRI and bone scintigraphy. *Eur Radiol* 2011; **21**: 2604-2617 [PMID: 21887484 DOI: 10.1007/s00330-011-2221-4]

16 **Liu T**, Xu JY, Xu W, Bai YR, Yan WL, Yang HL. Fluorine-18 deoxyglucose positron emission tomography, magnetic resonance imaging and bone scintigraphy for the diagnosis of bone metastases in patients with lung cancer: which one is the best?--a meta-analysis. *Clin Oncol* (R Coll Radiol) 2011; **23**: 350-358 [PMID: 21094027 DOI: 10.1016/j.clon.2010.10.002]

17 **Kaijzel EL**, Snoeks TJ, Buijs JT, van der Pluijm G, Löwik CW.

Multimodal imaging and treatment of bone metastasis. *Clin Exp Metastasis* 2009; **26**: 371-379 [PMID: 18941911 DOI: 10.1007/s10585-008-9217-8]

18 **Snoeks TJ**, Khmelinskii A, Lelieveldt BP, Kaijzel EL, Löwik CW. Optical advances in skeletal imaging applied to bone metastases. *Bone* 2011; **48**: 106-114 [PMID: 20688203 DOI: 10.1016/j.bone.2010.07.027]

19 **Gralow JR**, Biermann JS, Farooki A, Fornier MN, Gagel RF, Kumar R, Litsas G, McKay R, Podoloff DA, Srinivas S, Van Poznak CH. NCCN Task Force Report: Bone Health In Cancer Care. *J Natl Compr Canc Netw* 2013; **11** Suppl 3: S1-S50; quiz S51 [PMID: 23997241]

P- Reviewer: Boy C, Kara PO, Sakamoto A
S- Editor: Tian YL **L- Editor**: A **E- Editor**: Jiao XK

World Journal of Radiology

Submit a Manuscript: http://www.wjgnet.com/esps/
Help Desk: http://www.wjgnet.com/esps/helpdesk.aspx
DOI: 10.4329/wjr.v7.i8.212

World J Radiol 2015 August 28; 7(8): 212-219
ISSN 1949-8470 (online)

ORIGINAL ARTICLE

Basic study

Development of biodegradable radiopaque microsphere for arterial embolization-a pig study

Yi-Sheng Liu, Xi-Zhang Lin, Hong-Ming Tsai, Hung-Wen Tsai, Guan-Cheng Chen, Syuan-Fong Chen, Jui-Wen Kang, Chen-Miao Chou, Chiung-Yu Chen

Yi-Sheng Liu, Hong-Ming Tsai, Chen-Miao Chou, Department of Radiology, College of Medicine, National Cheng Kung University, Tainan 704, Taiwan

Xi-Zhang Lin, Guan-Cheng Chen, Syuan-Fong Chen, Jui-Wen Kang, Chiung-Yu Chen, Department of Internal Medicine, College of Medicine, National Cheng Kung University, Tainan 704, Taiwan

Hung-Wen Tsai, Department of Pathology, College of Medicine, National Cheng Kung University, Tainan 704, Taiwan

Author contributions: Lin XZ, Chen CY and Liu YS designed research; Liu YS, Chen GC, Chen SF and Kang JW performed research; Tsai HW contributed pathology reading; Lin XZ and Chen CY analyzed data; Chen CY and Liu YS wrote paper; all authors contributed to this paper.

Supported by The National Cheng-Kung University Hospital, No. NCKUH-102-01003.

Institutional review board statement: The experiment was approved by the ethical committee of the animal center of National Cheng Kung University (IACUC approval No. 102046).

Institutional animal care and use committee statement: The experiment was approved by the ethical committee of the animal center of National Cheng Kung University (IACUC approval No. 102046).

Conflict-of-interest statement: No potential conflicts of interest relevant to this article were reported.

Data sharing statement: No additional data are available.

Correspondence to: Chiung-Yu Chen, Medicinae Doctor, Department of Internal Medicine, College of Medicine, National Cheng Kung University, #138 Sheng-Li Road, Tainan 704, Taiwan. chiungyu@mail.ncku.edu.tw
Telephone: +886-6-2353535-2689
Fax: +886-6-2347270

Received: May 3, 2015
Peer-review started: May 3, 2015
First decision: June 18, 2015
Revised: July 7, 2015
Accepted: July 29, 2015
Article in press: August 3, 2015
Published online: August 28, 2015

Abstract

AIM: To develop a new type of calibrated, biodegradable, and imaging detectable microsphere and evaluated its embolization safety and efficacy on pig's liver and spleen.

METHODS: Six kinds of pharmaceutical excipient were combined and atomized to form our microsphere. Twenty-four male Lanyu pigs weighing 25-30 kg were used. The arteries of spleen and liver were embolized with Gelfoam, Embosphere, or our microsphere. The serum biochemical tests, computed tomography (CT), liver perfusion scan, and tissue microscopy examination were done to evaluate the safety and efficacy of embolization.

RESULTS: Radiopaque microspheres with a size ranging from 300 to 400 μm were produced. Embolization of hepatic and splenic artery of pigs with our microsphere significantly reduced the blood flow of liver and resulted in splenic infarction. The follow-up CT imaging and the microscopic examination showed intraarterial degradation of Gelfoam and microsphere. The blood tests

demonstrated insignificant changes with regards to liver and renal functions.

CONCLUSION: Our microspheres, with the unique characteristics, can be used for transcatheter arterial embolization with effects equivalent to or better than Gelfoam and Embosphere in pigs.

Key words: Atomization; Pharmaceutical excipient; Microsphere; Arterial embolization

Core tip: Transcatheter arterial embolization (TAE) is the treatment of choice for intermediate stage hepatocellular carcinoma. Various embolization materials have been designed for this purpose. By using atomization technique and a mixture of pharmaceutical excipient, we developed a new type of calibrated, biodegradable, and imaging detectable microsphere. We proved that our microspheres, with the unique characteristics, can be used for TAE with effects equivalent to or better than Gelfoam and Embosphere in pigs.

Liu YS, Lin XZ, Tsai HM, Tsai HW, Chen GC, Chen SF, Kang JW, Chou CM, Chen CY. Development of biodegradable radiopaque microsphere for arterial embolization-a pig study. *World J Radiol* 2015; 7(8): 212-219 Available from: URL: http://www.wjgnet.com/1949-8470/full/v7/i8/212.htm DOI: http://dx.doi.org/10.4329/wjr.v7.i8.212

INTRODUCTION

Hepatocellular carcinoma (HCC), the most common primary liver cancer, is the sixth most commonly diagnosed malignancy worldwide[1]. It is also the third leading cause of cancer-related mortality[1]. Conventional transcatheter arterial chemoembolization (cTACE) stands for the treatment of choice for Barcelona Clinic Liver Cancer stage B HCC[2,3]. By introducing embolic agents through an angio-catheter into the blood vessel, transcatheter arterial embolization (TAE) occludes tumor feeding vessels and thereby results in tumor shrinkage[4,5]. By adding chemotoxic agent(s) to the embolic materials, the cTACE evolved into more a controlled delivery of chemotherapy in the form of drug-eluting bead transcatheter arterial chemoembolization (DEB-TACE)[6].

Commercially available embolic materials include metallic coils, oils (lipiodol), non-spherical particles (Gelfoam) and microspheres (Embosphere, DC Bead and Hepasphere)[7]. As a tumor may recanalize the occluded vessels or form new vessels, repeated TAE is required in order to control tumor growth and a biodegradable embolic material allowing for the re-catheterization of previously embolized vessels is therefore, ideally preferred. Gelfoam is the only commercially available biodegradable embolic material at this time; however, it is non-spherical which makes it unable to precisely control the level of embolization[8].

Calibrated microspheres allow the radiologist to choose the size of microspheres according to the size of the targeting vessels. The DEB-TACE using drug-loaded microspheres showed less systemic toxicity and drug-related side-effects as compared to the cTACE[9]. However, both the Hepasphere and the DC Bead are not biodegradable, and it is reported that the long-term presence of DC Bead microspheres containing a potentially harmful drug in the body elicits chronic inflammation and thus causes more tissue injury[10]. Furthermore, these microspheres including the Embosphere are not radiopaque and interventional radiologists can only estimate the devascularization through an angiography, but do not know the precise site of occlusion of the injected microspheres[11].

To develop a new type of spherical, biodegradable, imaging detectable, and drug-loadable embolic material is therefore crucial in order to improve the efficacy of tumor embolization treatment. A biodegradable excipient able to be formulated with chemotoxic agent(s) and radiopaque contrast with suitable consistency will be a candidate of material to construct a microsphere for drug delivery and vascular embolization. Atomizing technique which breaks up bulk liquids into droplets can be applied to produce particles of desired shape, size, and density. In this study, we constructed a biodegradable radiopaque microsphere by atomizing a mixture of pharmaceutical excipient and conducted arterial embolization study in pigs in an attempt to explore a new microsphere that fulfills the above requirements for arterial embolization of HCC.

MATERIALS AND METHODS

Design of animal study

The experiment was conducted after the approval of the ethical committee of the animal center of our university and in accordance with the guidelines set forth by the Agriculture Council of Taiwan on animal care. The animal protocol was designed to minimize pain or discomfort to the animals. The animals were acclimatized to laboratory conditions (23 ℃, 12 h/12 h light/dark, 50% humidity, ad libitum access to food and water) during experimentation. Twenty-four male Lanyu pigs weighing 25-30 kg were included in the study. Arterial embolization of the liver with concomitant partial embolization of the spleen was used to test our newly developed embolic microsphere. Two other commonly used embolic materials for cTACE-Gelfoam and Embosphere were used for comparison. To better understand the acute and midterm effect of the embolic materials on pigs while avoid the potential anesthesia effects on pigs, blood tests were only checked on the day before embolization, 1 and 25 d after the embolization. To observe the evolutional change of our microsphere, non-enhanced CT scans were performed

on Day 4, 12, and 25 after the embolization. To estimate the blockade extent of liver blood flow by embolization materials, CT perfusion scans were performed on the pigs without embolization and immediately after embolization. All the animals were sacrificed 28 d after the embolization to examine the pathological changes in liver and/or spleen relating to embolization.

Manufacture of new microsphere

We combined several kinds of excipient from the handbook of pharmaceutical excipient to construct an excipient possessing suitable consistency for embolization. The excipient that we used included Lipiodol, Cetyl alcohol, Glycol monostearate, Stearyl acid, Polycaprolactone, and Cholesterol. All these materials are biodegradable and water insoluble. All these excipients were solid at room and body temperature, and become self-emulsifying oils at 65 ℃. Such a characteristic allowed us to melt and atomize it to make it into microsphere. In brief, the atomization procedure included a pressure type atomization technique for mass production of microspheres and a high frequency resonated technique to produce microspheres with a specific range of size. The size of microspheres was further examined by using a scanning electron microscope. With an aim to embolize intrahepatic arteries, microspheres with sizes of 300 to 450 μm were selected for the following embolization experiment.

Procedures of arterial embolization

The animals were fasted overnight and given free access to water. They were premedicated with intramuscular injection of Atropine (Sintong, Taoyuan, Taiwan) 0.02 mg/kg, Xylazine (Bayer, Leverkusen, Germany) 0.1 mL/kg, and Zoletil 50 (Virbac, Carros, France) 10 mg/kg. Following endotracheal intubation, the animals were anesthetized by using Propofol 12-20 mg/kg per hour (Tongchou, Taipei, Taiwan) intravenous injection or Isoflurane (Baxter, Guayama, United States) 1%-3% 200 mL/kg per minute inhalation throughout the operation. All animals were subjected to celiac artery angiography before the embolization. The procedure was performed with a femoral approach by using the Seldinger technique. After placing a 4-F introducer sheath (Cordis, Roden, the Netherlands), a 2.7-F microcatheter catheter (Progreat, Terumo, Tokyo, Japan) was used to catheterize the hepatic proper artery for liver embolization and one of the branches of splenic artery for splenic embolization because complete embolization of spleen caused a significant morbidity and mortality. As many embolization materials were introduced as possible and the end point of the procedure was to obtain blood flow stasis of the selected hepatic and splenic arteries.

Blood tests

By using intramuscular injection of Xylazine (Bayer, Leverkusen, Germany) 0.1 mL/kg and Zoletil 50 (Virbac, Carros, France) 10 mg/kg to anesthetize pig, serum samples were obtained on the day before embolization and 1 and 25 d after the embolization. Serum levels of blood urea nitrogen (BUN), creatinine, aspartate aminotransferase (AST), alanine aminotransferase (ALT), and total bilirubin were analyzed by using D and P modular analyzer (Roche, Mannheim, Germany).

Computed tomography

Each pig was anesthetized when undergoing computed tomography (CT) scanning and liver perfusion study. CT scanning and perfusion study was performed by a 128-section multidetector CT scanner (Definition Flash, Siemens Medical Systems; Erlangen, Germany). A dynamic study of the selected area was performed in a single breath hold at the end of expiration at a static table position. A total of 50 mL of nonionic iodinated contrast medium was injected at a rate of 5 mL/s, through an 18-gauge intravenous cannula. The liver blood volume (mL/100 mL) and the time that the liver started to be enhanced by contrast (time to start, second) were used to estimate the immediate embolization effects on liver perfusion.

Histological examinations

All animals were euthanized by barbiturate overdose (intravenous injection, 150 mg/kg pentobarbital sodium) for tissue collection. The transected liver and spleen harvested on the day of sacrifice were immediately fixed in a 10% formalin, sectioned, and stained with hematoxylin-eosin to investigate the changes of embolized arteries and peripheral tissues of both the spleen and liver.

Statistical analysis

The blood test results and the CT perfusion index between each group of pigs undergoing different treatments were analyzed by using one way ANOVA with LSD post-hoc test. A P value of < 0.05 was considered to be statistically significant.

RESULTS

New microsphere

As shown in Figure 1, microspheres with a size ranging from 300 to 400 μm were successfully produced. The size and shape were comparable to the current commercially used microsphere-Embosphere. Furthermore, due to radiopaque lipiodol being contained in our excipient mixture, our microsphere was different from the Embosphere in that it was radiopaque under fluoroscopy (Figure 2).

Transcatheter arterial embolizationof liver and spleen

Figure 3A presents the angiography of the liver of pig. As there were no liver tumors, embolization materials were injected into the hepatic proper artery to embolize bilateral intrahepatic arteries. Besides the liver, we also

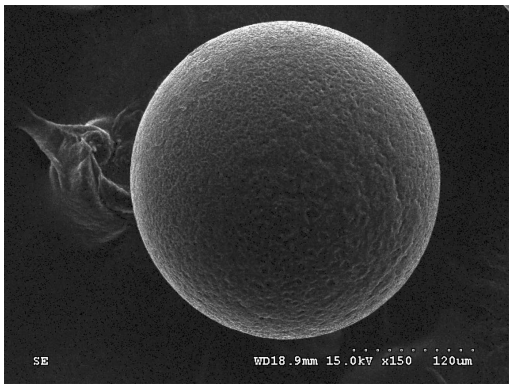

Figure 1 The microspheres in scanning electron microscope with a magnification of 150 ×.

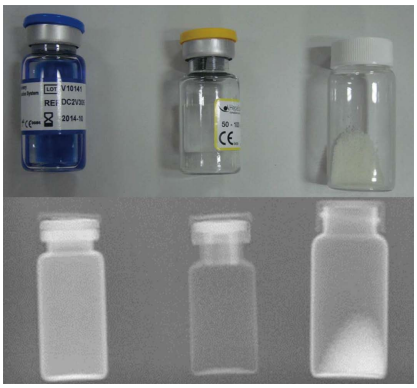

Figure 2 The gross appearance and fluoroscopy picture of DC bead (left), Hepasphere (middle), and our microsphere (right).

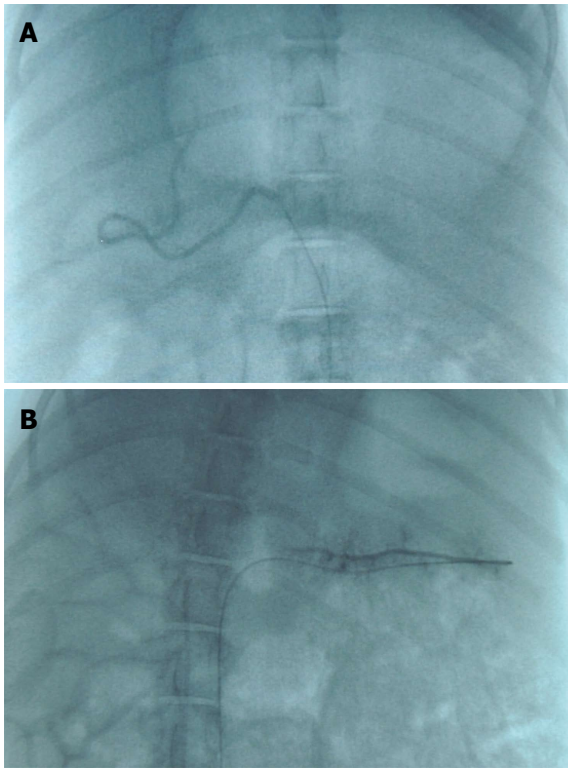

Figure 3 The angiography of hepatic artery (A) and splenic artery (B).

embolized one of the branches of splenic artery to test the embolization effect on spleen (Figure 3B).

Serum biochemical test

The blood tests confirmed the safety of the new microsphere based on our pig embolization experiment (Table 1). Similar to pigs embolized by Embosphere or Gelfoam, our microsphere embolization only caused mild increases in the serum levels of BUN, AST and ALT on the day after embolization and all returned to baseline at the end of experiment. Although the serum creatinine levels were higher in pigs receiving Gelfoam embolization on Day 25, the embolization did not cause any biochemical abnormality with regards to pig liver and the kidneys among groups embolized by different materials.

CT perfusion imaging and study

As shown in Table 2, the embolization effect of our microsphere was comparable to that of Embosphere and Gelfoam, in that all showed a significant reduction of perfused liver blood volume and a delayed contrast enhancement of the liver. The liver perfusion scan further demonstrated areas in the liver with a reduced blood flow after embolization (Figure 4).

CT imaging

As shown in Figure 5, the CT imaging showed retention of lipiodol in the liver after embolization by using our microsphere which faded away gradually in the subsequent follow up imaging. In contrast, both Embosphere and Gelfoam are radiolucent and there was no hyperintensity area found in the liver of pigs embolized with either one of them.

Pathology examination

Although the ingredients we used for our microsphere were all pharmaceutical excipient, the possible liver toxicity caused by such mixture can be a concern and was checked at first. Microscopically, the liver lobules did not have a significant pathology change after embolization with any of the three embolization materials (Figure 6). Infarction with shrinkage of the embolized part of spleen was noted in the pigs that underwent Embosphere and our microsphere embolization (Figure 7A and B) but grossly normal, in pigs embolized with Gelfoam (Figure 7C). Upon microscopic examination, partial degradation of our microsphere and Gelfoam with peripheral leukocyte infiltration within and around the embolized splenic vessels was observed which was in contrast to the presence of intact Embosphere within the embolized vessels (Figure 8). The different severity of splenic infarction among gelfoam, embosphere, and our microsphere may be therefore, caused by the selection of arterial branch on TAE rather than the character of embolization materials *per se*.

DISCUSSION

In this study, we successfully manufactured a micros-

Table 1 Sequential changes of biochemical tests before and after embolization

	Day 0			Day 1			Day 25		
	Gelfoam (n = 8)	Embosphere (n = 8)	Microsphere (n = 8)	Gelfoam (n = 8)	Embosphere (n = 8)	Microsphere (n = 8)	Gelfoam (n = 7)	Embosphere (n = 8)	Microsphere (n = 8)
AST	27.8 ± 15.3	24.4 ± 9.9	29.5 ± 12.3	56.4 ± 30.8[a,c]	34.9 ± 16.7[a]	103.0 ± 80.4[b]	23.1 ± 10.5	30.1 ± 20.6	35.4 ± 10.8
ALT	48.3 ± 23.9	34.8 ± 12.1	44.4 ± 20.6	58.9 ± 20.1	46.4 ± 17.3	51.5 ± 26.7	34.3 ± 19.6[a,c]	22.8 ± 12.6[c]	40.8 ± 17.0[c]
T-BIL	0.38 ± 0.15	0.40 ± 0.23	0.39 ± 0.15	0.29 ± 0.20	0.73 ± 1.00	0.68 ± 0.58	0.40 ± 0.14	0.39 ± 0.22	0.56 ± 0.34
BUN	12.1 ± 11.6	8.7 ± 6.4	8.5 ± 3.5	19.4 ± 9.4	18.3 ± 8.5	16.4 ± 9.2	8.7 ± 7.2	7.2 ± 4.1	10.5 ± 4.6
Cr	0.85 ± 0.19	0.75 ± 0.27	0.81 ± 0.21	0.84 ± 0.17	0.73 ± 0.28	0.86 ± 0.25	1.03 ± 0.26	0.86 ± 0.33	0.91 ± 0.18

[a,c]P < 0.05 by one way ANOVA test with LSD post-hoc test. AST: Aspartate aminotransferase; ALT: Alanine aminotransferase; T-BIL: Total bilirubin; BUN: Blood urea nitrogen; Cr: Creatinine.

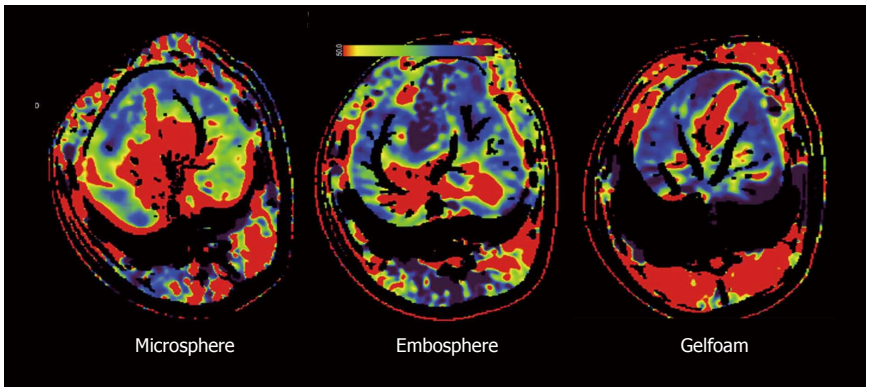

Figure 4 The liver perfusion scan after our microsphere, Embosphere, or Gelfoam embolization showing blood flow reduced areas (green to blue areas) over the periphery of liver.

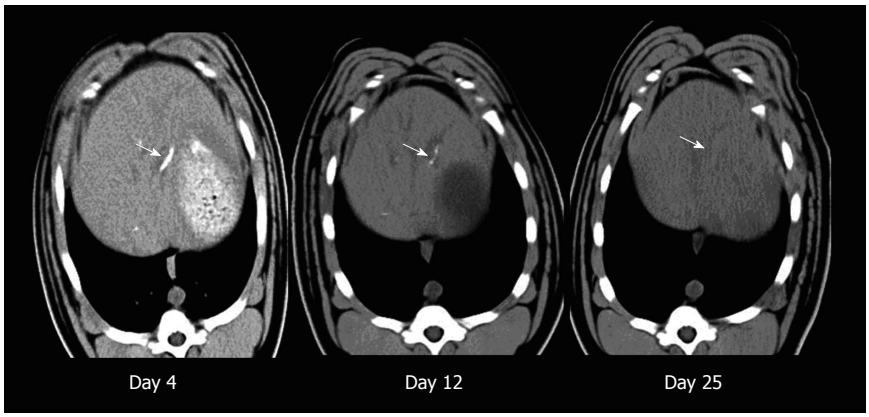

Figure 5 Serial non-enhanced computed tomography scans of pig's liver taken on 4, 12, and 25 d after the microsphere embolization showing its radiopaque characteristic and the gradual fade along with time (white arrow).

phere by atomizing mixture of pharmaceutical excipient. By using pig model, our microsphere was proven to be as safe and effective as currently used embolization materials-Embosphere and Gelfoam. Our microsphere was similar to Gelfoam in that it was biodegradable and Embosphere in that it was calibrated. Besides, our microsphere was radiopaque which can help radiologists to observe and monitor the entire embolization process.

Because the liver has dual blood supply coming from both portal vein and hepatic artery, arterial embolization by using commercial embolization materials or our microsphere did not cause any significant pathological or serum biochemical changes. The efficacy of embolization can only be investigated from the reduced blood flow of liver on CT perfusion imaging and the extent of splenic infarction after embolization of splenic artery. Based on these two findings, our microsphere was proven to be as effective as Embosphere and Gelfoam.

The size and the accurate caliber range of embolization microspheres is important to correctly deliver it to tumoral or peritumoral vessels. Drug-eluting or simple particles of 100-500 μm size are delivered into

Table 2 Hemodynamic changes of liver before and after embolization

Treatment	Non-embolized (n = 3)	Embosphere (n = 3)	Microsphere (n = 2)	Gelfoam (n = 2)
Blood volume[1]	12.75 ± 0.69	9.60 ± 1.48	9.42 ± 0.24	10.22 ± 1.24
Mean decrease		3.16 ± 0.82	3.33 ± 0.73	2.54 ± 0.82
P value		0.008	0.004	0.021
Time to Start[2]	11.40 ± 1.57	15.44 ± 2.10	15.91 ± 0.39	15.44 ± 1.74
Mean delay		4.04 ± 1.33	4.51 ± 1.19	4.04 ± 1.33
P value		0.023	0.009	0.023

[1]Blood volume estimated by arterial enhancement; [2]Time elapsed from contrast injection to the beginning of arterial enhancement; Data was expressed as mean ± SD; *P* value: Embolized group *vs* non-embolized group by one way ANOVA test with LSD post-hoc test.

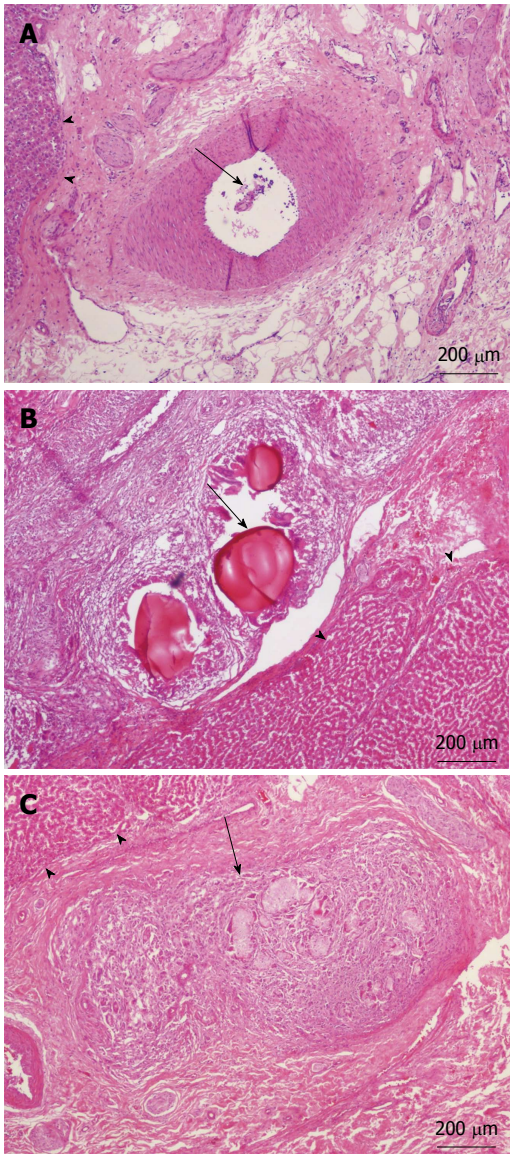

Figure 6 Microscopic findings of liver showing intraarterial embolization materials (black arrow) and intact peripheral liver lobules (black arrow heads) after Gelfoam (A), Embosphere (B), or our microsphere (C) embolization (H-E stain, original magnification × 40).

medium-sized vessels that irrigate tumor nodules with the aim of producing ischemia and finally exposing tumor cells to high concentrations of cytotoxic agents. Particles more than 500 μm occlude tumor feeding vessels and cause ischemia of both tumor and peritumoral liver[12]. By applying the atomizing technique, we were able to manufacture microspheres with a narrow size distribution as other calibrated materials such as DC-bead does using a microfluidics technique.

Drug eluting beads significantly reduced the peak plasma concentration of chemotoxic drug when compared with cTACE[13] and therefore, DEB-TACE has a lower frequency of adverse events than cTACE[14]. The mechanism of drug elution is attributed to an ionic exchange process between the hydrogel sulfonate or carboxyl counter ions of bead and anionic drug moieties[15,16]. Such a characteristic has limited the selection of chemotoxic drug to only drugs with anionic moieties. Excipient is a pharmacologically inactive substance and it can be formulated with the active gradient of a medication to give it a suitable consistency or form to a drug. Our microsphere was constructed by a mixture of excipient and thus has a greater potential to combine with various chemotoxic agents for cTACE.

Visualization of the microspheres during embolization would allow radiologists to investigate microsphere distribution within the tumor and liver and to evaluate as to whether distribution is homogeneous in the vasculature and whether the entire target tissue is embolized. All of this information regarding the distribution of the microsphere can be further correlated with the outcome of patients and would be extremely valuable to support the optimization of embolization protocols for a given type and size of tumor. Owning to the fact that lipiodol was included in our formulation of excipient, our microsphere therefore has an additional advantage over the currently used microsphere (*i.e.*, Embosphere and DC-bead) in that it was visible under fluoroscopy.

Gelfoam is the only commercially available biodegradable embolic material at this time; however, it is not spherical and thus unable to accurately control the level of embolization. For temporary embolization such as repeated TAE designated for controlling tumor growth, a biodegradable embolic material clearly preferred. Our microsphere was manufactured by biodegradable excipient. As evidenced by the histology examination and serial follow up CT scan, our microsphere was proven to be biodegradable and was therefore, a more

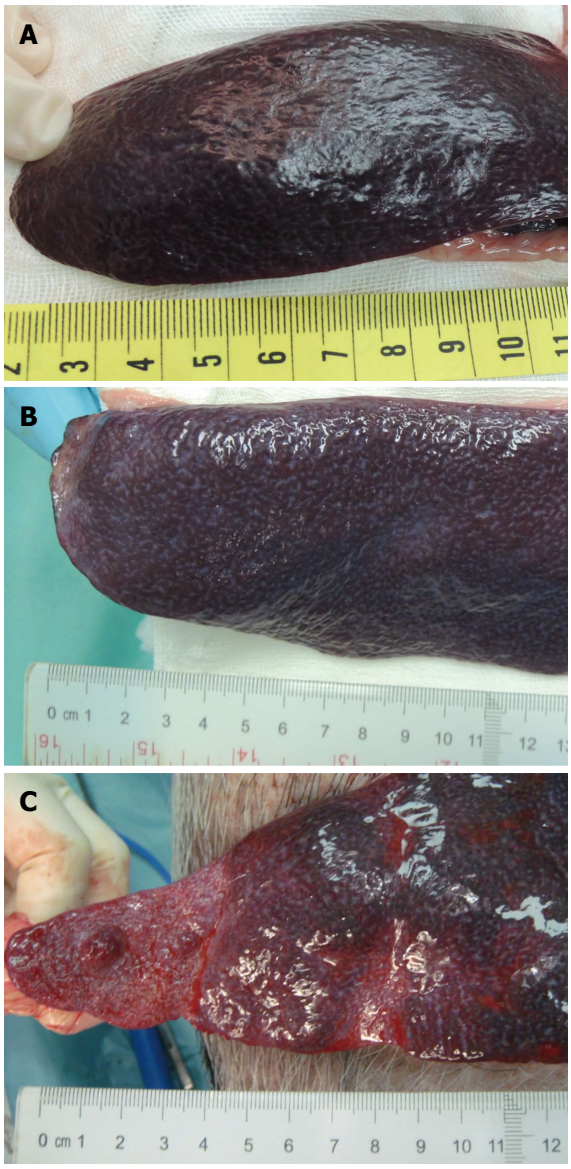

Figure 7 Gross appearance of spleen after Gelfoam (A), Embosphere (B), or our microsphere (C) embolization showing various degree of infarction over the distal end of spleen.

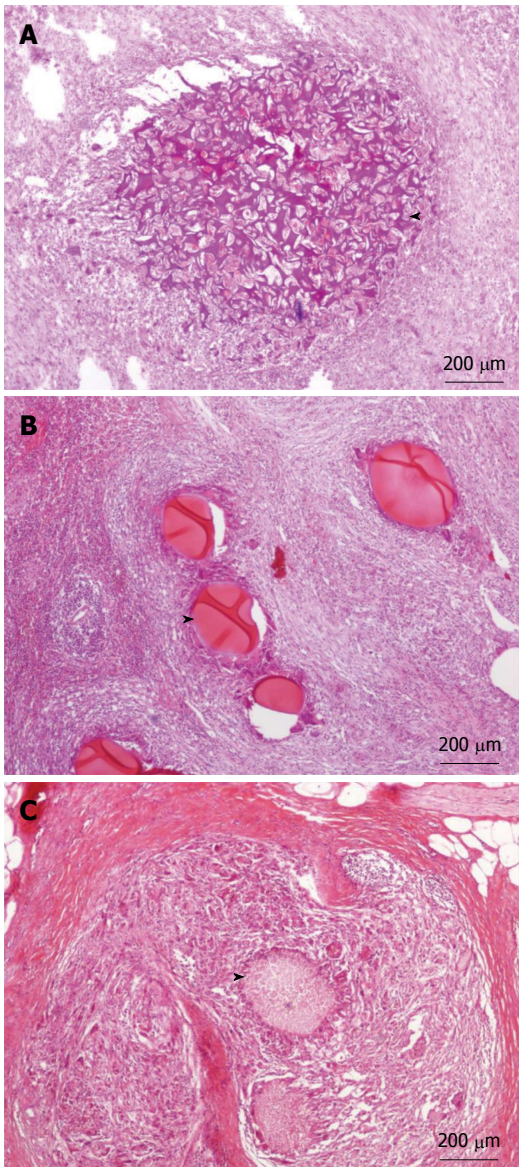

Figure 8 Microscopic findings of spleen showing intraarterial embolization materials (arrow heads) and periarterial reactions after Gelfoam (A), Embosphere (B), or our microsphere (C) embolization (H-E stain, original magnification × 40). Note the degrading Gelfoam and our microsphere and the intact Embosphere at 28 d after the embolization.

advantageous embolization material than Embosphere.

Although our microsphere has been proven to be useful for transcatheter arterial embolization in a pig model, the detailed physical properties such as rigidity to compression and *in vivo* deformation have not been studied. Deformation of microsphere in arteries and micro-catheters may lead to a more distal occlusion, and thus it is crucial when choosing a optimal sized microsphere to embolized targeted arteries[11]. In addition, we have not added chemotoxic agent to microsphere to evaluate the rate of drug eluting as it may complicate the evaluation of adverse effect of our microsphere if its safety has not been proved in advance. Studies regarding to these properties of our new microsphere are now ongoing.

In summary, our microspheres possess the characteristics of calibrated, radiopaque, and biodegradable and we proved their efficacy for TAE is equal to or better than Gelfoam and Embosphere.

COMMENTS

Background

Conventional transcatheter arterial chemoembolization (TACE) stands for the treatment of choice for Barcelona Clinic Liver Cancer stage B hepatocellular carcinoma (HCC). Drug-eluting bead transcatheter arterial chemoembolization controls the delivery of chemotoxic agent and reduces the side effects of chemotherapy. Biodegradable embolic material allows for the re-catheterization of embolized vessels and therefore, repetitive TACE. Calibrated microspheres allow the radiologist to choose the size of microspheres according to the size of the targeting vessels. Currently, there is no commercial microsphere that fulfills the above characteristics of an ideal embolization material.

Research frontiers

The authors constructed a biodegradable radiopaque microsphere by atomizing a mixture of pharmaceutical excipient. The conducted arterial embolization

study in pigs in an attempt to explore a new microsphere that fulfills the above requirements for arterial embolization of HCC.

Innovations and breakthroughs

Unlike DC-bead using a microfluidics technique to produce calibrated microsphere, the authors applied atomizing technique to manufacture microspheres with a narrow size distribution. The authors' microsphere was constructed by a mixture of excipient and thus has a greater potential to combine with various chemotoxic agents than the currently developed drug-eluting beads which uses ionic exchange process between the bead and anionic drug moieties. As evidenced by the histology examination and serial follow up CT scan, the authors' microsphere was proven to be biodegradable and was therefore, a more advantageous embolization material than Embosphere. By using pig model, their microsphere was proven to be as safe and effective as currently used embolization materials-Embosphere and Gelfoam.

Applications

Before applying the microsphere to patients with HCC, studies for the detailed physical properties such as rigidity to compression and *in vivo* deformation of microsphere and the rate of drug eluting from microsphere would be required. However, the study has demonstrated a brand new way and idea to produce embolization material for future arterial embolization.

Terminology

Atomization is a technique which breaks up bulk liquids into droplets and has been applied to produce particles of desired shape, size, and density. Excipient is a pharmacologically inactive substance and it can be formulated with the active gradient of a medication to give it a suitable consistency or form to a drug.

Peer-review

This is a very well designed animal study. This biodegradable radiopaque microsphere has a high potential to develop into a commercial product used for transcatheter arterial embolization of HCC.

REFERENCES

1 **Jemal A**, Bray F, Center MM, Ferlay J, Ward E, Forman D. Global cancer statistics. *CA Cancer J Clin* 2011; **61**: 69-90 [PMID: 21296855 DOI: 10.3322/caac.20107]

2 **Bruix J**, Sherman M. Management of hepatocellular carcinoma. *Hepatology* 2005; **42**: 1208-1236 [PMID: 16250051 DOI: 10.1002/hep.20933]

3 **Bruix J**, Sherman M, Llovet JM, Beaugrand M, Lencioni R, Burroughs AK, Christensen E, Pagliaro L, Colombo M, Rodés J. Clinical management of hepatocellular carcinoma. Conclusions of the Barcelona-2000 EASL conference. European Association for the Study of the Liver. *J Hepatol* 2001; **35**: 421-430 [PMID: 11592607]

4 **Oerlemans C**, Seevinck PR, van de Maat GH, Boulkhrif H, Bakker CJ, Hennink WE, Nijsen JF. Alginate-lanthanide microspheres for MRI-guided embolotherapy. *Acta Biomater* 2013; **9**: 4681-4687 [PMID: 22947326 DOI: 10.1016/j.actbio.2012.08.038]

5 **Kang MJ**, Park JM, Choi WS, Lee J, Kwak BK, Lee J. Highly spherical and deformable chitosan microspheres for arterial embolization. *Chem Pharm Bull* (Tokyo) 2010; **58**: 288-292 [PMID: 20190430]

6 **Salem R**, Lewandowski RJ. Chemoembolization and radioembolization for hepatocellular carcinoma. *Clin Gastroenterol Hepatol* 2013; **11**: 604-611; quiz e43- e44 [PMID: 23357493 DOI: 10.1016/j.cgh.2012.12.039]

7 **Weng L**, Rostamzadeh P, Nooryshokry N, Le HC, Golzarian J. In vitro and in vivo evaluation of biodegradable embolic microspheres with tunable anticancer drug release. *Acta Biomater* 2013; **9**: 6823-6833 [PMID: 23419554 DOI: 10.1016/j.actbio.2013.02.017]

8 **Laurent A**, Wassef M, Chapot R, Houdart E, Merland JJ. Location of vessel occlusion of calibrated tris-acryl gelatin microspheres for tumor and arteriovenous malformation embolization. *J Vasc Interv Radiol* 2004; **15**: 491-496 [PMID: 15126660]

9 **Namur J**, Citron SJ, Sellers MT, Dupuis MH, Wassef M, Manfait M, Laurent A. Embolization of hepatocellular carcinoma with drug-eluting beads: doxorubicin tissue concentration and distribution in patient liver explants. *J Hepatol* 2011; **55**: 1332-1338 [PMID: 21703190 DOI: 10.1016/j.jhep.2011.03.024]

10 **Lammer J**, Malagari K, Vogl T, Pilleul F, Denys A, Watkinson A, Pitton M, Sergent G, Pfammatter T, Terraz S, Benhamou Y, Avajon Y, Gruenberger T, Pomoni M, Langenberger H,Schuchmann M, Dumortier J, Mueller C, Chevallier P, Lencioni R. Prospective randomized study of doxorubicin-eluting-bead embolization in the treatment of hepatocellular carcinoma: results of the PRECISION V study. *Cardiovasc Intervent Radiol* 2010; **33**: 41-52 [PMID: 19908093 DOI: 10.1007/s00270-009-9711-7]

11 **Laurent A**. Microspheres and nonspherical particles for embolization. *Tech Vasc Interv Radiol* 2007; **10**: 248-256 [PMID: 18572137 DOI: 10.1053/j.tvir.2008.03.010]

12 **Sangro B**, Iñarrairaegui M, Bilbao JI. Radioembolization for hepatocellular carcinoma. *J Hepatol* 2012; **56**: 464-473 [PMID: 21816126 DOI: 10.1016/j.jhep.2011.07.012]

13 **Gonzalez MV**, Tang Y, Phillips GJ, Lloyd AW, Hall B, Stratford PW, Lewis AL. Doxorubicin eluting beads-2: methods for evaluating drug elution and in-vitro:in-vivo correlation. *J Mater Sci Mater Med* 2008; **19**: 767-775 [PMID: 17653626 DOI: 10.1007/s10856-006-0040-y]

14 **Vogl TJ**, Lammer J, Lencioni R, Malagari K, Watkinson A, Pilleul F, Denys A, Lee C. Liver, gastrointestinal, and cardiac toxicity in intermediate hepatocellular carcinoma treated with PRECISION TACE with drug-eluting beads: results from the PRECISION V randomized trial. *AJR Am J Roentgenol* 2011; **197**: W562- W570 [PMID: 21940527 DOI: 10.2214/AJR.10.4379]

15 **Lencioni R**, Crocetti L, Petruzzi P, Vignali C, Bozzi E, Della Pina C, Bargellini I, Cioni D, Oliveri F, De Simone P, Bartolozzi C, Brunetto M, Filipponi F. Doxorubicin-eluting bead-enhanced radiofrequency ablation of hepatocellular carcinoma: a pilot clinical study. *J Hepatol* 2008; **49**: 217-222 [PMID: 18486261 DOI: 10.1016/j.jhep.2008.03.021]

16 **Liu DM**, Kos S, Buczkowski A, Kee S, Munk PL, Klass D, Wasan E. Optimization of doxorubicin loading for superabsorbent polymer microspheres: in vitro analysis. *Cardiovasc Intervent Radiol* 2012; **35**: 391-398 [PMID: 21567274 DOI: 10.1007/s00270-011-0168-0]

P- Reviewer: Kim HC, Lau WY, Morris DL
S- Editor: Ji FF **L- Editor**: A **E- Editor**: Jiao XK

Published by **Baishideng Publishing Group Inc**
8226 Regency Drive, Pleasanton, CA 94588, USA
Telephone: +1-925-223-8242
Fax: +1-925-223-8243
E-mail: bpgoffice@wjgnet.com
Help Desk: http://www.wjgnet.com/esps/helpdesk.aspx
http://www.wjgnet.com